A modified spectral-domain model for nonlinear hydrostatic restoring force of heaving wave energy converters

Tan, Jian; Lavidas, George

Important note
To cite this publication, please use the final published version (if applicable).
Please check the document version above.

Research paper

A modified spectral-domain model for nonlinear hydrostatic restoring force of heaving wave energy converters

Jian Tan [*], George Lavidas

Faculty of Civil Engineering and Geosciences, Delft University of Technology, Stevinweg, 1, 2628 CN, Delft, The Netherlands

ARTICLE INFO

ABSTRACT

A modified spectral-domain (SD) model is introduced in this study to address the nonlinear hydrostatic restoring force for heaving wave energy converters (WECs) with non-uniform cross-sectional areas. Distinguished from previous SD models, the modified SD model collectively includes the effects of incident wave elevation and buoy displacement, through the utilization of the multi-variate stochastic linearization method. The proposed SD model is verified against results obtained from a corresponding nonlinear time-domain (TD) model. Subsequently, a comprehensive comparison is carried out between the modified SD model, the other two existing SD models and the linear frequency-domain (FD) model. The nonlinear TD model is considered as the accuracy reference in this comparison. Various environmental and operational inputs, such as sea states, Power Take-Off (PTO) parameters, and buoy drafts, are systematically taken into account in the comparison. Additionally, the computational efficiency of each model is evaluated.

The results suggest that the modified SD model demonstrates significantly enhanced accuracy in cases where hydrostatic force nonlinearity intensifies, compared to the existing SD models and the FD model. Throughout the entire domain of the simulation cases, the maximum relative error of the modified SD model to the nonlinear TD model is below 5 %, while it is 20 % for the FD model and approximately 15 % for the two existing SD models. Moreover, the modeling accuracy of the FD model and existing SD models could be strongly disturbed by the variation of the environmental and operational inputs. Comparatively, the modified SD model is associated with much more stable accuracy. Nevertheless, the modified SD model only requires a modest increase in computational load compared to the FD model and existing SD models and it is still thousands of times faster than the nonlinear TD model.

1. Introduction

In the context of renewable energy, ocean wave energy stands out as an environmentally friendly, energy-dense, and globally abundant resource (Lavidas and Venugopal, 2017; Guillou et al., 2020; Jin and Greaves, 2021). Despite its immense potential to contribute to the ongoing energy transition, the development of wave energy converters (WECs) currently lags behind other marine renewable energy technologies, such as offshore wind turbines (Soukissian et al., 2023; Taveira-Pinto et al., 2020; Martinez and Iglesias, 2022). This discrepancy primarily arises from the comparatively higher cost of energy associated with WECs in comparison to other renewable technologies (Guo and Ringwood, 2021; Lavidas and Blok, 2021b,a; Tan et al., 2021a). To overcome this hurdle and unlock the full potential of wave energy, continuous refinement of WEC designs is imperative.

Over the past few decades, numerical modeling approaches have emerged as pivotal tools in the early-stage design and optimization of WECs (Guo and Ringwood, 2021). Offering a compelling advantage of reduced economic and time investments compared to experiments or sea trials, numerical modeling serves as an effective means to unveil the dynamic behavior and power performance of various WEC concepts. By fostering a deeper understanding of the complex interplay between design parameters and performance outcomes, numerical representations of WEC can pave the way for iterative advancements in pursuing more economical and efficient wave energy conversion technologies.

Various numerical modeling approaches can be applied to model WECs. The three most utilized modeling approaches consist of frequency-domain (FD) modeling, time-domain (TD) modeling based on Cummins equation, and fully nonlinear Computational Fluid Dynamics (CFD) modeling (Anon, 2016). These modeling approaches are associated with different fidelity while the computational efficiency varies significantly. For instance, CFD modeling is often utilized to estimate the behavior of WECs in extreme wave climates, mainly contributing to survivability evaluation rather than power performance

---

* Corresponding author.
E-mail address: j.tan-2@tudelft.nl (J. Tan).

estimation, focusing on short-time duration simulations (Ransley et al., 2017). Comparatively, the power production assessment of WECs necessarily involves a large number of operation conditions due to the notable variation of wave climates. In this case, the numerical tools with high computational efficiency, namely FD models and TD models, are commonly applied (Pecher, 2017).

In the field of WECs, a vast number of FD models and TD models are established relying on linear potential flow theory assuming idealized fluid, as extensively reviewed in Penalba Retes et al. (2015). Using simplified boundary conditions covering the mean free surface and mean wetted surface of the floating structure, the hydrodynamic coefficients can be efficiently derived through the linear potential flow theory. These frequency-dependent coefficients could describe the incoming wave force, radiation force, and diffraction force subjected to the floating structure in different wave conditions. Combined with the mass property, the hydrostatic property, and other external forces, the obtained hydrodynamic coefficients can facilitate the construction of the equation of motion in the frequency domain. In the FD modeling, all responses of the analyzed system are expressed as frequency-dependent components, and the whole system has to be fully linear (Pastor and Liu, 2014). In mild operation regions, both the wave elevation and the motion amplitude of the floater can be considered small. In this case, the nonlinearity of the WEC system is far from being pronounced, leading to adequate accuracy of FD modeling approaches (Li and Yu, 2012).

The TD modeling approach can be used to derive the time-dependent dynamic responses of the system. This approach is formulated based on the Cummins equation (Cummins et al., 1962) in which the memory effects of radiation force are described. In principle, with identical hydrodynamic coefficients as part of the modeling, FD modeling and TD modeling are expected to deliver the same output, regardless of numerical errors in solving the partial differential equations in the TD models. However, the structure of the TD modeling inherently allows for the inclusion of additional time-dependent equations of nonlinear effects. A range of influential nonlinear effects have been incorporated into the TD modeling and have been validated, including nonlinear mooring force, Power Take-Off (PTO) force saturation, end-stop mechanism, and viscous drag force (Giorgi and Ringwood, 2018b,a; Anon, 2016; Babarit et al., 2012; Tan et al., 2022c,d, 2023a). As a consequence, TD domain modeling is widely acknowledged as an approach associated with improved accuracy compared with the FD modeling approach, particularly in situations with higher wave elevations and larger floater motions. Despite providing higher fidelity compared to FD models, the normalized computational time demanded by the TD modeling approach appears to be substantially higher than that of the corresponding FD models (Tan et al., 2022b). The increased computational loads result from numerical integration schemes applied in TD modeling to solve partial differential equations at each time step (Ricci et al., 2008).

In recent years, the spectral-domain (SD) modeling approach has received notable research interest, as a newly emerging alternative to the FD or TD modeling method (Folley, 2016). SD modeling has high computational efficiency since it is established based on the extension of FD modeling. At the same time, SD modeling enables the incorporation of nonlinear effects by applying stochastic linearization, which enhances the modeling accuracy in comparison to the FD modeling approach. Hence, integrating adequate accuracy with high computational efficiency facilitates the SD modeling approach strongly to fit scenarios requiring a substantial number of simulations, such as power production estimation of WECs. The development of the SD modeling approach for WECs began with a model addressing quadratic damping and excitation force decoupling in oscillating surge WECs (Folley and Whittaker, 2010). The established SD model was validated against the corresponding nonlinear TD mode, and a good agreement was observed with regard to power capture and power spectral density of the responses of the WEC. Subsequent studies extended the coverage

of SD modeling to more nonlinear effects involved in wave energy conversion. In Folley and Whittaker (2013), a SD model was developed for an oscillating water column to include the nonlinear damping term, and the proposed model was validated by experimental data. In Silva (2019), Silva et al. (2020), da Silva et al. (2020), Spanos et al. (2018), Tan et al. (2022b), the linearized representations of a range of relevant nonlinear components were obtained and incorporated into the SD modeling, including the end-stop mechanism, nonlinear mooring stiffness, Coulomb damping, Morison equation, PTO force capping and partial overlap of linear generators. In Bonfanti and Giorgi (2022), Bonfanti and Sirigu (2023), a SD model was thoroughly developed for a gyroscopic-type WEC, in which the nonlinear effects, including Coulomb damping, PTO force saturation and end-stop mechanism, were collectively incorporated. More recently, SD modeling was further developed in Tan et al. (2023b), Tan and Laguna (2023) to represent the entire wave-to-wire process of WECs, in which the WEC system responses in not only the hydrodynamic phase but also the electric phase can be modeled.

Existing WECs differ significantly in the geometrical design. For WECs with non-uniform cross-sectional area, the hydrostatic force exerted on the WEC hull would be nonlinear with respect to the displacement of the WEC. The nonlinearity of the hydrostatic force has a notable impact on the performance of WECs (Zurkinden et al., 2014; Ji et al., 2020; Wolgamot and Fitzgerald, 2015; Coe and Bull, 2015; Lawson et al., 2014a). In Zurkinden et al. (2014), the dynamics of a semi-spherical point absorber WEC were numerically and experimentally investigated. The results indicated that the consideration of the nonlinear hydrostatic behaviors in the numerical model reduces the prediction error by up to 150%. In Ji et al. (2020), a numerical study was performed for a two-body heaving point absorber WEC, in which different shapes of the upper buoy were considered for identifying the impact of the nonlinear hydrostatic force. The results of linear and nonlinear hydrostatic representations in the numerical models were compared, with FD and TD models being employed respectively for linear and nonlinear ones. It concluded that the nonlinear hydrostatic force has a considerable effect on the dynamic performance of the buoy, and it is essential to include the effect for accurately estimating the loads and power performance of WECs with non-uniform shaped buoys. Additionally, the effects of the nonlinear hydrostatic force of WECs have also been demonstrated in Wolgamot and Fitzgerald (2015), Coe and Bull (2015), Lawson et al. (2014a), which implies the importance of taking it into account in numerical modeling. However, the above-mentioned studies were all using the TD modeling approach to address the nonlinear hydrostatic behavior. In the pursuit of a more computationally efficient numerical tool, the research efforts were devoted to incorporating the nonlinear hydrostatic effect into SD modeling. However, limited to the single-variate stochastic linearization method, nonlinear effects can only be addressed when they are related to one variable. Therefore, in Gunawardane et al. (2017), Silva et al. (2020), the SD modeling was developed to cover the nonlinear hydrostatic force for spherical point absorber WECs, but the hydrostatic force was simplified to be a nonlinear function only related to the displacement of the buoy without considering the variation of wave elevation. In a follow-up study (Tan et al., 2022a), the hydrostatic force was expressed to be a function of the relative displacement between the buoy displacement and the wave elevation. As a result, the linearization could be conducted by taking the relative displacement as the variable. However, there is still a remaining cross term of the wave elevation and the relative displacement in the expression of the hydrostatic force. To make the single-variate stochastic linearization method applicable for the cross term, a compromise was made by assuming that the contribution resulting from the relative displacement is negligible compared to the wave elevation. It is noted that the simplifications in these SD models could ease the complexity of stochastic linearization of the hydrostatic force. However, it also raises concerns about reducing the
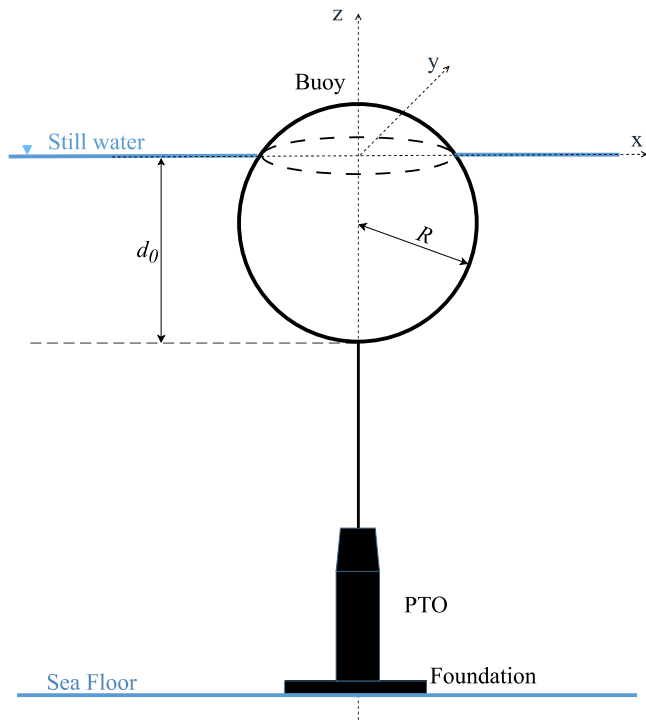
Fig. 1. Schematic of the spherical heaving point absorber with a bottom founded PTO system.

accuracy, particularly during significant relative movement between the buoy and wave elevation.

To enhance accuracy, a modified SD model addressing the nonlinear hydrostatic restoring force is presented in this study, and the bi-variate stochastic linearization method is utilized. This marks the first application of this method in the context of SD modeling of WECs. The primary objective is to achieve a more realistic representation of the nonlinear hydrostatic restoring force compared to previously reported hydrostatic SD models relying on single-variate linearization. The WEC concept is considered to be a generic heaving point absorber WEC. To better demonstrate the modeling performance, a significantly non-uniform buoy shape, namely the spherical geometry, is defined for the floater of the WEC. Besides, the corresponding nonlinear TD model is employed as a reference for verifying the estimation accuracy of SD modeling. Furthermore, the proposed SD model, the existing SD models, the linear FD model, and the nonlinear TD model are compared among each other. Various affecting factors are considered in the comparison, accounting for the significant wave height, the PTO parameters, and the buoy drafts. Both the modeling accuracy and the computational efficiency of different models are presented in the comparison.

2. WEC concept description

The WEC concept in this work is defined as a floating heaving point absorber, which is illustrated in Fig. 1. The geometry of the floating buoy is considered as a sphere with a radius of 2.5 m. The mass of the buoy is assumed to be the same as that of the displaced water by the buoy.

In wave energy conversion, the PTO system serves as a crucial linkage between the moving buoy and the electrical generator. It is acknowledged that various types of PTO systems exist, differing in operating principles, size, efficiency, etc (Prado and Polinder, 2013; Tan et al., 2022d, 2021b). However, considering the scope of the work, the PTO component in the WEC is simplified to function in a fully linear manner. Comprehensive studies on integrating more realistic

representations of PTO systems into SD modeling can be found in Tan et al. (2022b), Silva et al. (2020), Tan et al. (2023b), Tan and Laguna (2023).

3. Numerical modeling

3.1. Time-domain modeling

In this study the WEC is assumed to oscillate in heave motion, the numerical model is only discussed for this degree of freedom. According to the Cummins equation (Cummins et al., 1962), the equation of motion of a floating rigid buoy can be described in the time domain as

$$[m + M_r(\infty)]\ddot{z}(t) + \int_{-\infty}^{t} K_{rad}(t - \tau)\dot{z}(\tau)d\tau = F_e(t) + F_{pto}(t) + F_{hs}(t) \quad (1)$$

where m and $M_r(\infty)$ are the body mass and the added mass evaluated at the infinite frequency, and K_{rad} is the radiation impulse function; z, $\dot{z}$ and $\ddot{z}$ stand for the displacement, the velocity and the acceleration of the rigid body; F_e, F_{pto} and F_{hs} denote the wave excitation force, PTO force and hydrostatic restoring force respectively; t stands for the time. The convolution term in the right hand of the equation describes the memory effect of the radiation force.

In the TD modeling, the time-averaged power absorption of the WEC can be expressed as

$$\overline{P}_{ab} = \frac{1}{T} \int_{t=0}^{T} -F_{pto}(t)\dot{z}(t)dt \quad (2)$$

where T represents the assessed time duration.

3.2. Frequency-domain modeling

If the floating body is assumed to undergo harmonic oscillation subjected to regular waves and linear external forces, (1) could be rewritten in the form of complex amplitudes in the frequency domain Falnes (2003), Tan et al. (2020), Pastor and Liu (2014), as

$$\hat{F}_e(\omega) + \hat{F}_{hs,lin} = \hat{z}(\omega) \left\{ -\omega^2 \left[m + M_r(\omega) \right] + K_{pto} + i\omega \left[R_r(\omega) + R_{pto} \right] \right\} \quad (3)$$

where ω is the angular wave frequency; F_e is the amplitude of the excitation force, $R_r(\omega)$ and $M_r(\omega)$ are the radiation damping coefficient and the added mass of the buoy. K_{pto} and R_{pto} are the PTO damping and stiffness coefficient, and $\hat{z}$ is complex amplitude of the vertical displacement. $\hat{F}_{hs,lin}$ embodies the complex amplitude of the linear hydrostatic restoring force.

The excitation force, radiation damping and added mass are commonly derived by the boundary element method (Anon, 2016). The complex amplitude of the excitation force is expressed as

$$\hat{F}_e(\omega) = f_e e^{i\phi_{fe}(\omega)} \eta e^{i\phi_\eta(\omega)} \quad (4)$$

where f_e is the excitation force coefficient which is defined as the excitation force amplitude normalized to the incoming wave amplitude, η is the wave amplitude at the evaluated frequency component, ϕ_{fe} is the phase angle between the excitation force and incoming wave force, and ϕ_η is the phase angle of the incoming wave with regard to the reference point. The reference point in this paper is selected as the geometry center of the buoy.

As the complex amplitude of the displacement is derived for each frequency component, the power spectral density of the buoy displacement is calculated as

$$S_z(\omega) = \frac{1}{2} \frac{|\hat{z}(\omega)|^2}{\Delta\omega} \quad (5)$$

The variance of the displacement is calculated as

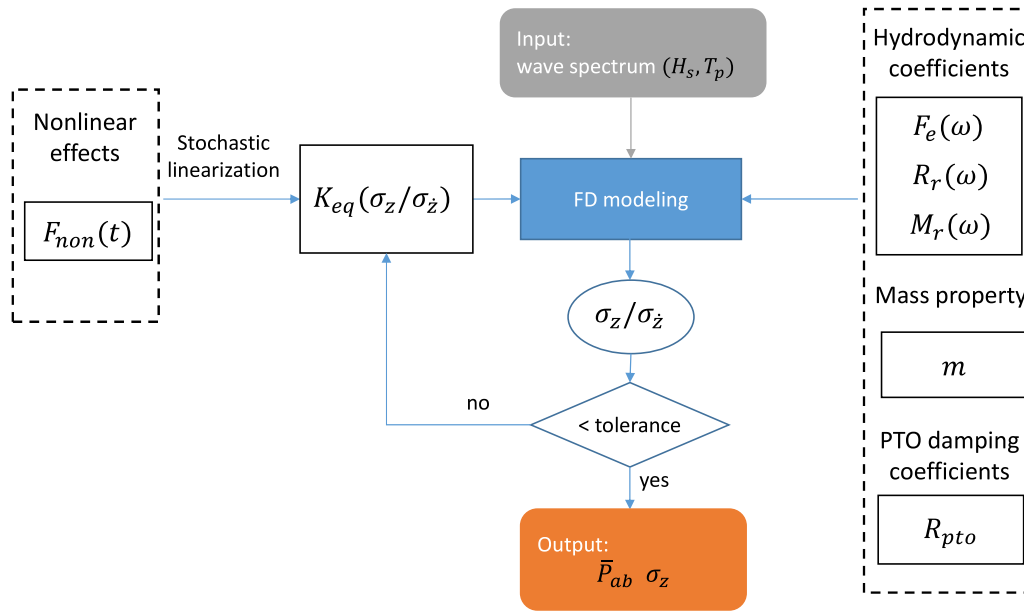$$\sigma_z^2 = \sum_{j=1}^{N} S_z(\omega_j)\Delta\omega \quad (6)$$

Fig. 2. Flowchart of implementing SD modeling for WECs.

The variance of the velocity can also be calculated following this way as

$$\sigma_{\dot{z}}^2 = \sum_{j=1}^{N} \frac{1}{2} |i\omega_j \hat{z}(\omega_j)|^2 \tag{7}$$

Subsequently, the mean absorbed power in FD modeling is derived as

$$\overline{P}_{ab} = R_{pto}\sigma_{\dot{z}}^2 \tag{8}$$

3.3. Spectral-domain modeling

3.3.1. Framework of spectral-domain modeling

The SD modeling approach is extended from the framework of the FD modeling, and the flowchart of implementing the SD modeling is illustrated in Fig. 2. The main difference between the FD and SD modeling approaches comes from the inclusion of the equivalent linearized coefficients, K_{eq}, which are used to represent the considered nonlinear force F_{non} in SD modeling. The coefficients are derived based on the stochastic linearization method, which will be detailed in the subsequent subsection.

As explained in Tan et al. (2022b), Folley and Whittaker (2010), the linearized coefficients in SD modeling are inherently expressed as related to the responses' standard deviation, which is unknown information before solving the system. In this case, an iteration scheme has to be applied in the computation, and the first guess of the standard deviation is taken from the results of the corresponding FD model. The iteration is terminated until the defined tolerance is reached. Upon the derived standard deviations of the WEC responses, (8) applies to the calculation of the absorbed power in SD modeling.

3.3.2. Stochastic linearization in SD modeling

A comprehensive demonstration of the stochastic linearization method, an integral component of probabilistic analysis of dynamic structures, can be found in Roberts and Spanos (2003). As described in Roberts and Spanos (2003), assuming a Gaussian process for a random system enables the stochastic linearization of nonlinearities. This approach simplifies the analysis of nonlinear dynamic systems by approximating them as equivalent linear systems.

The principle of stochastic linearization is to find an equivalent coefficient for replacing the nonlinear component in the system's equation of motion. In a stochastic process, the equivalent term is expected to balance the energy or power dissipation of the corresponding nonlinear effect. Despite the fact that this method has been employed and demonstrated in previous studies of the SD modeling for WECs (Folley, 2016; Folley and Whittaker, 2010), existing SD models are predominately constructed based on the single-variate stochastic linearization method. This approach is highly applicable to nonlinear functions involving only one variable, such as the quadratic drag term (Silva et al., 2020). A few previous studies have considered the inclusion of nonlinear effects involving multiple variables in SD modeling (Bonfanti and Sirigu, 2023; Bonfanti and Giorgi, 2022). However, due to the lack of application of the multi-variate stochastic linearization method, these studies essentially simplified the multi-variate cases to fit the single-variate stochastic linearization framework. Although these studies have provided significant and inspiring insights into incorporating more complex nonlinearities into SD modeling, they are inherently associated with strong limitations. For example, three compromised approaches were employed in Bonfanti and Sirigu (2023) to address multi-variate nonlinear functions. The first way was to neglect the correlation between variables, which directly simplifies the multi-variate scenarios. This can be a highly strong assumption for related variables. The second approach was to numerically search the statistical contribution of the nonlinear effects without deriving a closed-form solution, which could significantly increase the computational burden. Third, integration domains were split to represent one variable by another in each specific integration area, allowing the single-variate stochastic method to apply within each integration domain. This approach is limited to very specific nonlinear functions. Therefore, the dependence on the single-variate stochastic method hinders the expansion of SD modeling to cover more generic multi-variate nonlinearities in the context of WECs. However, in other engineering disciplines, such as control engineering, the method of stochastic linearization has been recently proposed and applied to address multi-variate nonlinear functions (Brahma and Ossareh, 2021, 2018). The proposed method is introduced in the current work to address the bi-variate function of the hydrostatic restoring force of WECs. This work could also contribute to the examination of the applicability of the proposed method in the context of WECs. The derivations of stochastic linearization for single-variate and bi-variate cases are briefly outlined in the following text. Additional details are

available in Folley and Whittaker (2010, 2013), Folley (2016) concerning the linearization of single-variate nonlinearities and in Brahma and Ossareh (2021, 2018) for multi-variate nonlinearities.

- Single-variate case
  A single-variate nonlinear function F_{non} can be expressed as

$$F_{non} = g(u) \tag{9}$$

where u is the input variable and g embodies a nonlinear function. Let its linear equivalent, denoted as $f_e(u)$, be expressed as

$$f_e(u) = Nu + M \tag{10}$$

here, a and b serve as quasi-linear coefficients, while $g(u)$ represents a general nonlinear function with respect to u. The resulting error in the linearization is given by

$$\epsilon = g(u) - Nu - M \tag{11}$$

Statistically, the expected value of the error squared, denoted by $\langle \epsilon^2 \rangle$, is calculated as

$$\langle \epsilon^2 \rangle = \langle (g(u) - Nu - M)^2 \rangle \tag{12}$$

where $\langle \cdot \rangle$ denotes the expected value of a function. Minimizing the squared error requires N and M to satisfy the following conditions:

$$\frac{\partial}{\partial N} \langle \epsilon^2 \rangle = 0 \quad \text{and} \quad \frac{\partial}{\partial M} \langle \epsilon^2 \rangle = 0 \tag{13}$$

Solving (13) yields the solutions

$$N = \langle \frac{\partial g(u)}{\partial u} \rangle \quad \text{and} \quad M = \langle g(u) \rangle \tag{14}$$

The linearized equivalent function is expected to make the same energy or power dissipation as the exact nonlinear force does in the dynamic system. With the stochastic linearization, the expected value of the reactive energy or the power of the nonlinear force can be expressed as

$$\begin{aligned} J &= \langle F_{non} u \rangle \\ &\approx \langle f_e(u) u \rangle \\ &= \langle (Nu + M) u \rangle \\ &= \langle Nu^2 \rangle + \langle M \rangle \langle u \rangle \end{aligned} \tag{15}$$

If the variable u adheres to a zero-mean Gaussian distribution, the last term $\langle M \rangle \langle u \rangle$ can be removed. In this sense, only N needs to be determined in the stochastic linearization.

- Bi-variate case
  A nonlinear function F_{non} of two variables u_1 and u_2 can be expressed in a generic form as

$$F_{non} = f(u_1, u_2) \tag{16}$$

in which $f(\cdot)$ stands for a nonlinear function; and $u_1(t), u_2(t)$ represent the input variables to the function. The variables can be expressed in the form of a vector as $\mathbf{u}(t) = [u_1(t) \ u_2(t)]^T$. Stochastic linearization could give an approximation to the nonlinear function as

$$V \approx \mathbf{N}\mathbf{u} + M \tag{17}$$

where N represents the linearized coefficients with being a constant vector $\mathbf{N} = [N_1 \ N_2]$, and M is a constant. If the elements in the vector $u(t)$ are jointly Gaussian processes, as has been proved in Brahma and Ossareh (2021, 2018), the linearized coefficients are derived as

$$\mathbf{N} = \langle \nabla f(\mathbf{u}) \rangle \tag{18}$$

where ∇ means the gradient operator, and it is given as

$$\nabla = \begin{bmatrix} \frac{\partial}{\partial u_1} & \frac{\partial}{\partial u_2} \end{bmatrix}^T \tag{19}$$

3.4. Representations of the hydrostatic restoring force

The focus of the present work is specifically on the hydrostatic restoring force of heaving WECs. The hydrostatic restoring force is defined as the balance between the hydrostatic force and the gravitational force acting on the floating buoy (Giorgi and Ringwood, 2017). Depending on the modeling fidelity, the hydrostatic restoring force can be represented in various forms. Three different representations are depicted in Fig. 3, and they are detailed in the following text.

- *Representation 1: instantaneous free surface and instantaneous wetted surface*
  In the nonlinear hydrostatic restoring force model, the assumptions of the mean free surface and the mean wetted surface are lifted. This condition can be illustrated in Fig. 3(a) where both the instantaneous wave elevation and the floating buoy are displaced from their mean positions. As detailed in Giorgi et al. (2016), Giorgi and Ringwood (2017), the hydrostatic force is computed by integrating static pressure over the wetted surface of the buoy. In this way, the instantaneous hydrostatic restoring force can be determined using

$$F_{hs}(t) = -\iint_{S_w(t)} P_{st} \mathbf{n} dS_w - mg \tag{20}$$

where $S_w(t)$ and P_{st} embody the wetted surface of the buoy and static pressure at the position of interest; $\mathbf{n}$ represents the normal vector on the surface of the buoy. Applying Gaussian divergence to the integral in (20), the instantaneous hydrostatic restoring force F_{hs} can be rewritten as:

$$F_{hs}(t) = \rho g V_{sub}(t) - \rho g \Delta z A_{wp}(t) - mg \tag{21}$$

here, V_{sub} and A_{wp} represent the instantaneous submerged volume and water-plane area of the buoy, respectively. ρ is the water density, and g is the gravitational acceleration. The variables V_{sub} and A_{wp} are intricately linked to the incident wave elevation η and the buoy's heaving displacement z. The term Δz signifies the vertical distance from the water-plane area A_{wp} to the reference height $z = 0$. Assuming the device remains within operational bounds, Δz can be replaced by the wave elevation η. The hydrostatic restoring force can be expressed as a function of two variables—the incident wave elevation η and the buoy's displacement z as articulated in (22).

$$F_{hs}(z, \eta) = \rho g V_{sub}(z, \eta) - \rho g \eta A_{wp}(z, \eta) - mg \tag{22}$$

In the case of a floating spherical buoy, the volume of the displaced water and the water-plane area are expressed as

$$V_{sub}(z, \eta) = \pi \left[d_0 - (z - \eta) \right]^2 \left[R - \frac{d_0 - (z - \eta)}{3} \right] \tag{23}$$

$$A_{wp}(z, \eta) = \pi \left\{ R^2 - \left[d_0 - (z - \eta) - R \right]^2 \right\} \tag{24}$$

where R is the radius of the sphere and d_0 is the draft of the buoy at the still water level.

- *Representation 2: mean free surface and instantaneous wetted surface*
  This representation can be illustrated by Fig. 3(b), in which the effect of incident wave elevation is assumed to be negligible while including the instantaneous wetted surface of the floating buoy. In this sense, $\eta = 0$ can be substituted into (22), resulting in a simplified expression of the nonlinear hydrostatic restoring force as shown in (25).

$$F_{hs}(z, 0) = \rho g V_{sub}(z, 0) - mg \tag{25}$$

This representation simplifies the expression of the nonlinear hydrostatic restoring force to be a single-variate function purely depending on the buoy displacement.

Representation 1: instantaneous free surface + instantaneous wetted surface
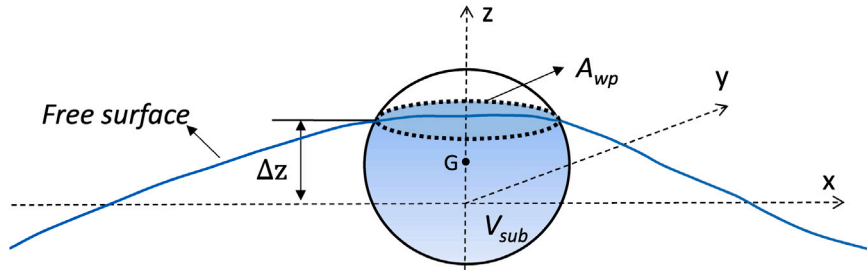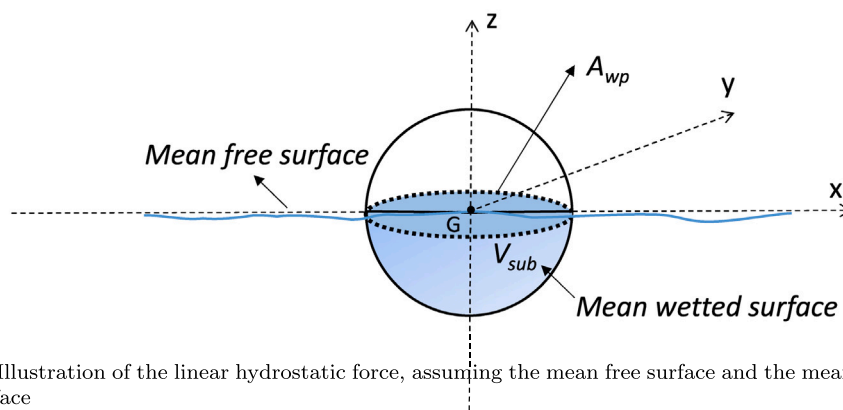
(a) Illustration of the nonlinear hydrostatic force, considering the instantaneous free surface and the instantaneous wetted surface. Δz represents the vertical distance from A_{wp} to the reference height $z = 0$.

Representation 2: mean free surface + instantaneous wetted surface
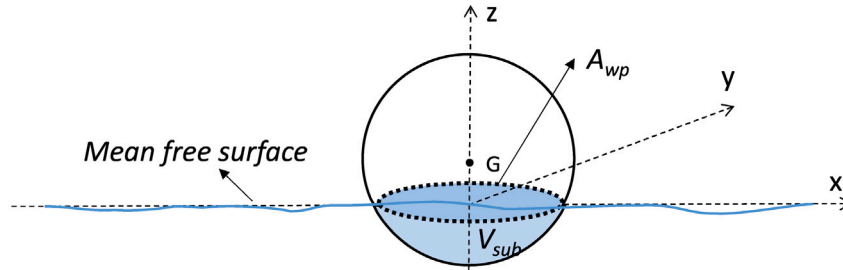
(b) Illustration of the nonlinear hydrostatic restoring force with instantaneous wetted surface, assuming the mean free surface

Representation 3: mean free surface + mean wetted surface

(c) Illustration of the linear hydrostatic force, assuming the mean free surface and the mean wetted surface

Fig. 3. Representations of the hydrostatic restoring force of a heaving buoy. A_{wp} and V_{sub} denote the water-plane area and the submerged volume of the floater; G represents the gravity center.

- *Representation 3: mean free surface and mean wetted surface*
  Fig. 3(c) describes the hydrostatic restoring force in a fully linear form, in which both the waves and the buoy's motion are considered sufficiently small. As a consequence, the assumptions of the mean free surface and the mean wetted surface of the buoy are made. Thus, the hydrostatic restoring force can be approximated by a constant hydrostatic stiffness coefficient $K_{lin,hs}$, expressed as

$$F_{hs,lin}(z) = K_{lin,hs} z \tag{26}$$

where $F_{hs,lin}$ represents the linear hydrostatic restoring force.

Fig. 4 visualizes the resulting hydrostatic restoring force of the heaving spherical buoy associated with the different representations. The buoy is excited to perform harmonic motion under regular waves,

in which different buoy displacement amplitudes, wave amplitudes and phase differences are implemented. The discrepancy in the obtained hydrostatic restoring force is evident among these representations.

3.5. Overview of existing modeling approaches

In prior studies, several modeling approaches have been used to address the hydrostatic restoring force acting on WECs. These approaches are elaborated in the subsequent text for comparison.

- *Nonlinear hydrostatic force in TD modeling* (NHF-TD)
  This approach corresponds to the representation 1. The TD modeling of WECs is established based on the Cummins equation, which is to be solved numerically. This structure inherently enables
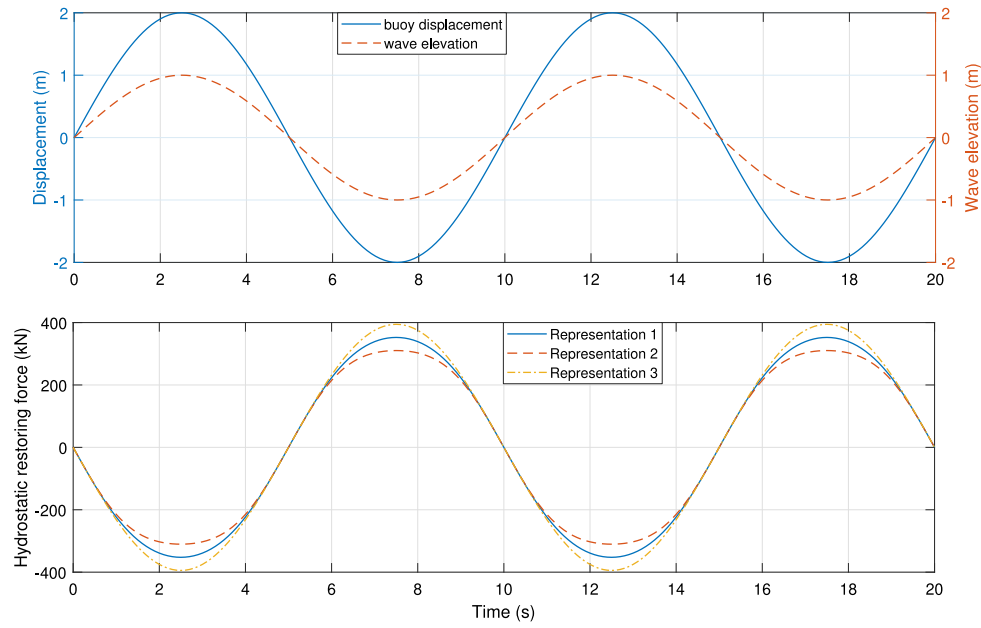
(a) The displacement and wave amplitudes are 2 m and 1 m. The phase difference between the wave elevation and the buoy displacement is 0
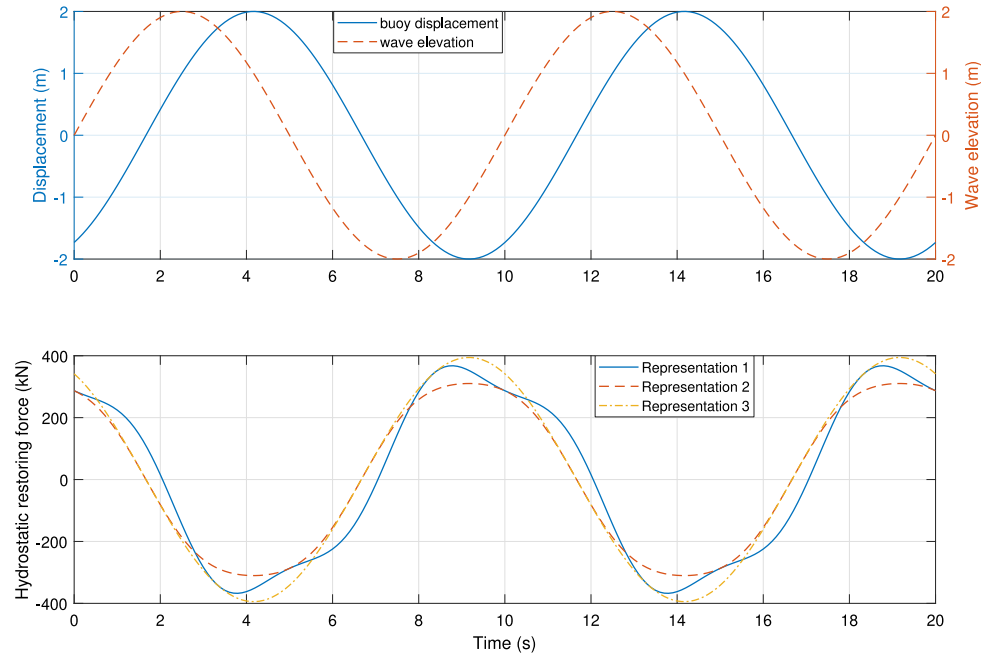
(b) The displacement and wave amplitudes are 1 m and 1.5 m. The phase difference between the wave elevation and the buoy displacement is $\pi/3$

Fig. 4. The profiles of the hydrostatic restoring force of the spherical buoy correspond to different representations under regular waves and harmonic motion of the buoy.

the inclusion of nonlinear effects by adding additional time-dependent terms. Thus, in the TD modeling approach, the expression of the nonlinear hydrostatic restoring force can be maintained in an exact form as given in (22). In this work, the nonlinear TD modeling is considered to be a reference for verifying other models.

- *Linear hydrostatic force in FD modeling* (LHF-FD)
  This approach corresponds to the representation 3. In FD modeling, the hydrostatic restoring force needs to be simplified to be a linear form. As shown in (26). The linear hydrostatic restoring stiffness is expressed as

$$K_{lin,hs} = -\rho g A_{wp}(0,0) \tag{27}$$

Assuming all the other components in the system are also linear, the equation of motion for the buoy can be expressed in FD modeling, as depicted in (3). Therefore, the motion of the buoy can be solved using the following expression:

$$\hat{z}(\omega) = \frac{\hat{F}_e(\omega)}{\left[-\omega^2(m + M_r(\omega)) + K_{pto} - K_{hs,lin}\right] + i\omega\left[R_r(\omega) + R_{pto}\right]} \tag{28}$$

This equation provides a response solution for the heaving displacement of the buoy in the frequency domain, where $\hat{z}(\omega)$ represents the complex amplitude of the heaving motion under the regular waves of an angular frequency of ω.

- *Single-variate linearization of hydrostatic force in SD modeling* (SLHF-SD)

  This approach corresponds to the representation 2. Different from conventional FD modeling which is fully linear, SD modeling could incorporate nonlinear effects through stochastic linearization. In several relevant studies (Silva et al., 2020; Gunawardane et al., 2017), the SD modeling approach was developed to address the nonlinear hydrostatic restoring force. In their models, the influence of the buoy displacement on the calculation of the hydrostatic force was included, but the assumption of the mean free surface was still applied. As shown in (14), the linearized representation of (25) for the SD modeling can be derived as

$$
\begin{aligned}
K_{eq} &= \langle \frac{\partial F_{hs}(z,0)}{\partial z} \rangle \\
&= \langle -\rho g A_{wp}(z,0) \rangle
\end{aligned}
\tag{29}
$$

The linearized coefficient K_{eq} can be further expressed as related to the standard deviation of the WEC response σ_z, and more details of the derivation are available in Appendix A. Subsequently, $K_{lin,hs}$ can be replaced with K_{eq} in (3), and the motion of the buoy is obtained as

$$
\hat{z}(\omega) = \frac{\hat{F}_e(\omega)}{\left[-\omega^2(m + M_r(\omega)) + K_{pto} - K_{eq} \right] + i\omega \left[R_r(\omega) + R_{pto} \right]}
\tag{30}
$$

- *Simplified bi-variate linearization of hydrostatic force in SD modeling* (SBLHF-SD)

  This approach corresponds to the representation 1. A simplified bi-variate linearization approach was proposed in Tan et al. (2022b) to incorporate the hydrostatic restoring force in SD modeling. In this approach, both the buoy displacement and the incident wave elevation are treated as variables in the linearization process of the hydrostatic restoring force. However, to ease the complexity of the linearization procedure, the correlation between the incident wave elevation and the buoy displacement is assumed to be negligible. This assumption will be elaborated upon in detail in the text above Eq. (38).

  In the method, a new variable, namely the relative displacement between the incident wave elevation η and the buoy displacement z, is introduced to express V_{sub} and A_{wp} in (22). The relative displacement is denoted as h which is defined as

$$
h(t) = z(t) - \eta(t)
\tag{31}
$$

At each wave frequency component, (31) can be expressed as

$$
\begin{aligned}
\text{Re}\{\hat{h}e^{i\omega t}\} &= \text{Re}\{\hat{z}e^{i\omega t}\} - \text{Re}\{\hat{\eta}e^{i\omega t}\} \\
&= \text{Re}\{(\hat{z} - \hat{\eta})e^{i\omega t}\}
\end{aligned}
\tag{32}
$$

Therefore, the complex amplitude of the relative displacement can be calculated as

$$
\hat{h}(\omega) = \hat{z}(\omega) - \hat{\eta}(\omega)
\tag{33}
$$

Subsequently, (22) can be rewritten as a function of the relative displacement as

$$
F_{hs}(h) = \rho g V_{sub}(h) - \rho g \eta A_{wp}(h) - mg
\tag{34}
$$

where V_{sub} and A_{wp} are the functions representing the submerged volume and cross-sectional area. Therefore, the hydrostatic restoring force can be separated into two parts. The first one F_{hs1} is a function of h, and another one F_{hs2} is a function of the wave elevation η and h, as

$$
F_{hs1}(h) = \rho g V_{sub}(h) - mg
\tag{35}
$$

$$
F_{hs2}(\eta, h) = -\rho g \eta A_{wp}(h)
\tag{36}
$$

According to Folley and Whittaker (2010), the linearized coefficients of (35) can be calculated as

$$
\begin{aligned}
K_{eq1} &= \langle \frac{\partial F_{hs1}(h)}{\partial h} \rangle \\
&= \rho g \langle \frac{\partial V_{sub}(h)}{\partial h} \rangle \\
&= \langle -\rho g A_{wp}(h) \rangle
\end{aligned}
\tag{37}
$$

It is seen that (36) is dependent on two variables. Assuming an uncorrelation between the two variables could simplify the stochastic linearization process to a single-variate case. Based on this assumption, it can be deduced that the relative variation of η is much larger than that of $A_{wp}(h)$ in (36) in the operational conditions of WECs. In this case, η is assumed to play a major role in the variation of F_{hs2}, and $A_{wp}(h)$ is treated as a constant in the stochastic linearization. Consequently (36) can be rewritten as

$$
F_{hs2}(\eta) = -\rho g \eta A_{wp}(h)
\tag{38}
$$

Subsequently, the linearization of (38) is calculated as

$$
\begin{aligned}
K_{eq2} &= \langle \frac{\partial F_{hs2}(\eta)}{\partial \eta} \rangle \\
&= \langle -\rho g A_{wp}(h) \rangle
\end{aligned}
\tag{39}
$$

These two linearized coefficients can be obtained following the derivation given in Appendix B, and then (3) is rewritten as

$$
\hat{F}_e + \hat{F}_{hs} = \hat{z} \left\{ \left[-\omega^2(m + M_r(\omega)) + K_{pto} \right] + i\omega \left[R_r(\omega) + R_{pto} \right] \right\}
\tag{40}
$$

The complex amplitude of the hydrostatic restoring force is expressed as

$$
\begin{aligned}
\hat{F}_{hs} &= \hat{F}_{hs1} + \hat{F}_{hs2} \\
&= K_{eq1}(\hat{z} - \hat{\eta}) + K_{eq2}\hat{\eta}
\end{aligned}
\tag{41}
$$

Subsequently, the motion of the buoy can be solved as

$$
\begin{aligned}
\hat{z}(\omega) &= \frac{\hat{F}_e - (K_{eq1} - K_{eq2})\hat{\eta}}{\left[-\omega^2(m + M_r(\omega)) + K_{pto} - K_{eq1} \right] + i\omega \left[R_r(\omega) + R_{pto} \right]} \\
&= \frac{\hat{F}_e}{\left[-\omega^2(m + M_r(\omega)) + K_{pto} - K_{eq1} \right] + i\omega \left[R_r(\omega) + R_{pto} \right]}
\end{aligned}
\tag{42}
$$

3.6. Modified SD model: Bi-variate linearization of hydrostatic force (BLHF-SD)

This approach also aligns with representation 1 in Fig. 3, while the simplification present in the SBLHF-SD model is not necessary here. To avoid the simplification in the SBLHF-SD model, the above-mentioned bi-variate stochastic linearization method is applied to address the nonlinear function (22). As the nonlinear function (22) is related to two variables η and z, the vector of the linearized coefficients for the hydrostatic restoring force can be derived according to (18) as

$$
\begin{bmatrix} K_{eq,\eta} \\ K_{eq,z} \end{bmatrix} = \left\langle \begin{bmatrix} \frac{\partial F_{hs}(z,\eta)}{\partial \eta} \\ \frac{\partial F_{hs}(z,\eta)}{\partial z} \end{bmatrix} \right\rangle
\tag{43}
$$

where $K_{eq,\eta}$ and $K_{eq,z}$ are the linearized coefficients respective to the variables η and z. Following the derivation provided in Appendix C, $K_{eq,\eta}$ and $K_{eq,z}$ can be expressed as related to the standard deviations of the WEC response and the wave elevation. Then, the hydrostatic restoring force in the modified SD model can be represented as

$$
\hat{F}_{hs} = K_{eq,\eta}\hat{\eta} + K_{eq,z}\hat{z}
\tag{44}
$$

Substituting (44) into (3) gives the solution to the motion response of the WEC system as

$$\hat{z}(\omega) = \frac{\hat{F}_e + K_{eq,\eta}\hat{\eta}}{\left[-\omega^2(m + M_r(\omega)) + K_{pto} - K_{eq,z}\right] + i\omega\left[R_r(\omega) + R_{pto}\right]} \tag{45}$$

4. Implementation of simulation

This study utilizes a representation of irregular waves formulated through the superposition of 500 individual harmonic wave components. The angular frequencies of these wave components are evenly distributed in the range from 0.05π to 4π rad/s. To mimic the stochastic characteristics of ocean waves, a random phase assumption is applied to these wave components. Additionally, the irregular wave states are modeled using the JONSWAP spectrum, with a peakedness factor set at 3.3. Theoretically, the modeling approaches discussed in this paper could also apply to other types of wave spectra and spectrum parameters (Folley, 2016; Folley and Whittaker, 2013).

The same set of hydrodynamic coefficients of the spherical floater is used for the construction of FD, SD, and TD modeling. These coefficients, namely $M_r(\omega)$, $R_r(\omega)$ and $f_e(\omega)$, are computed by an open-source boundary element method software Nemoh (Penalba et al., 2017). For TD modeling, a state-space approximation is used in this work to replace the convolution term shown in (1) since it is significantly computationally demanding. The frequency-domain identification method developed in Pérez and Fossen (2008) is applied to derive the state-space parameters. The ODE 45 solver embodied in MATLAB is used to solve the partial differential equation in TD modeling. The displacement and the velocity of the WEC are defined as zero in the initial condition. The simulation time duration and time step are defined as 100 times and 0.01 times the considered peak period T_p, respectively. To mitigate strong transient flow occurring at the initial simulation time, a ramp function is utilized in each TD simulation to avoid the drastic initial transient flow, and the ramp period lasts for the first 25 T_p (Lawson et al., 2014). Notably, the ramp time is excluded from the power performance analysis of the WEC. As the random phase assumption inevitably brings random errors, each simulation is repeatedly executed 30 times in TD modeling, with updating the random phase set every time, to obtain mean values. The framework of the applied TD model has been verified in previous work (Tan et al., 2022c, 2023b,a).

In the SD simulation, an iterative process has to be employed to solve the responses of the WEC. A convergence tolerance of 0.1% is defined in this process (Silva et al., 2020; Folley and Whittaker, 2013), ensuring accuracy and stability in the SD simulation results. Throughout the iterative process in this study, the standard deviation of the WEC displacement, as computed by FD modeling, serves as the initial guess of the standard deviation of the displacement. Subsequently, the revised responses, obtained through the equation of motion, are updated in each iteration, enabling the calculation of a new value for the standard deviation of the displacement σ_z^+. Following this, a refined approximation of σ_z is derived as a weighted sum of the previous estimate σ_z^- and the renewed estimate σ_z^+, expressed by:

$$\sigma_z = \kappa\sigma_z^+ + (1 - \kappa)\sigma_z^- \tag{46}$$

Here, κ represents the weighting factor. The refined approximation σ_u is then utilized to formulate an updated value of the equivalent linearized coefficient for the subsequent iteration. This iterative process continues until the difference between the previous and iterative values converges within a specified range. Convergence is verified for all simulation cases presented in this work.
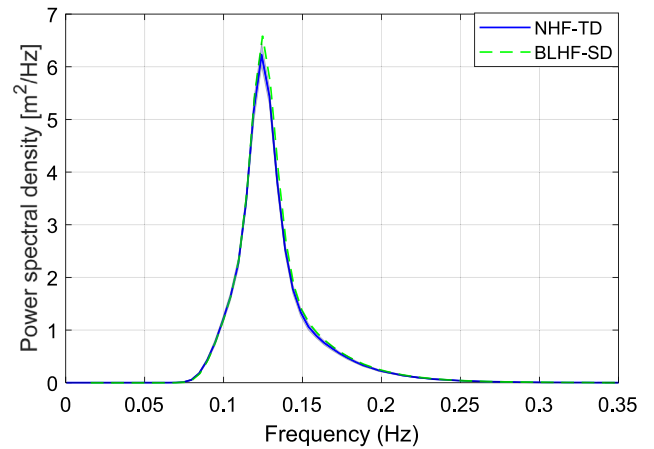

Fig. 5. The power spectral density of the displacement of the WEC ($H_s = 2.5$ m, $T_p = 8.0$ s and $B_{pto} = 150$ kNs/m). The shaded area is used to represent the standard deviation of the TD modeling results.

5. Results and discussion

5.1. Verification of BLHF-SD model

As a newly proposed numerical model, it is first essential to demonstrate the correctness of the BLHF-SD model. In this section, the verification of the BLHF-SD model is presented. The NHF-TD model is considered the verification reference here since it is inherently associated with higher modeling fidelity than the FD and SD models. Throughout the simulation, the buoy draft is considered 2.5 m which implies the semi-submerged sphere unless it is particularly specified.

Fig. 5 illustrates the comparison between the power spectral densities of displacement estimated by the NHF-TD model and those by the BLHF-SD model. Notably, the BLHF-SD model exhibits good agreement with the NHF-TD model across the entire range of evaluated frequency components. Only slight deviations can be observed in regions near the peak frequency of the wave state. This discrepancy can be attributed to higher wave amplitude components intensifying the nonlinearity of the hydrostatic restoring force. Fig. 6 shows the values of the standard deviation of the displacement estimated by the NHF-TD model and the BLHF-SD model, in which various sea states and several parameters of the PTO damping are taken into account. It is seen that these two models return highly close results of the standard deviation of the displacement over a variety of sea states. The difference between the results of the two models tends to increase with the significant wave height, while it is still at a low level of below 4.5% at a relatively powerful significant wave height, namely 4 m. Therefore, it is believed that the proposed BLHF-SD model is correctly implemented, and it demonstrates adequate accuracy in incorporating the effect of the nonlinear hydrostatic restoring force.

5.2. Modeling comparison

In this subsection, a comprehensive comparative analysis of modeling approaches addressing the hydrostatic restoring force is conducted. The analyzed models include the NHF-TD model, the LHF-FD model, the SLHF-SD model, the SBLHF-SD model, and the proposed BLHF-SD model. Various factors affecting the nonlinearity of the hydrostatic restoring force are considered for a thorough comparison. These factors encompass sea states, PTO control parameters, and buoy drafts. The relevance of modeling accuracy of different numerical models to these factors is demonstrated accordingly. A normalized power capture factor, namely the capture width ratio (CWR), is used to compare the accuracy of different models on the power estimate. The CWR is
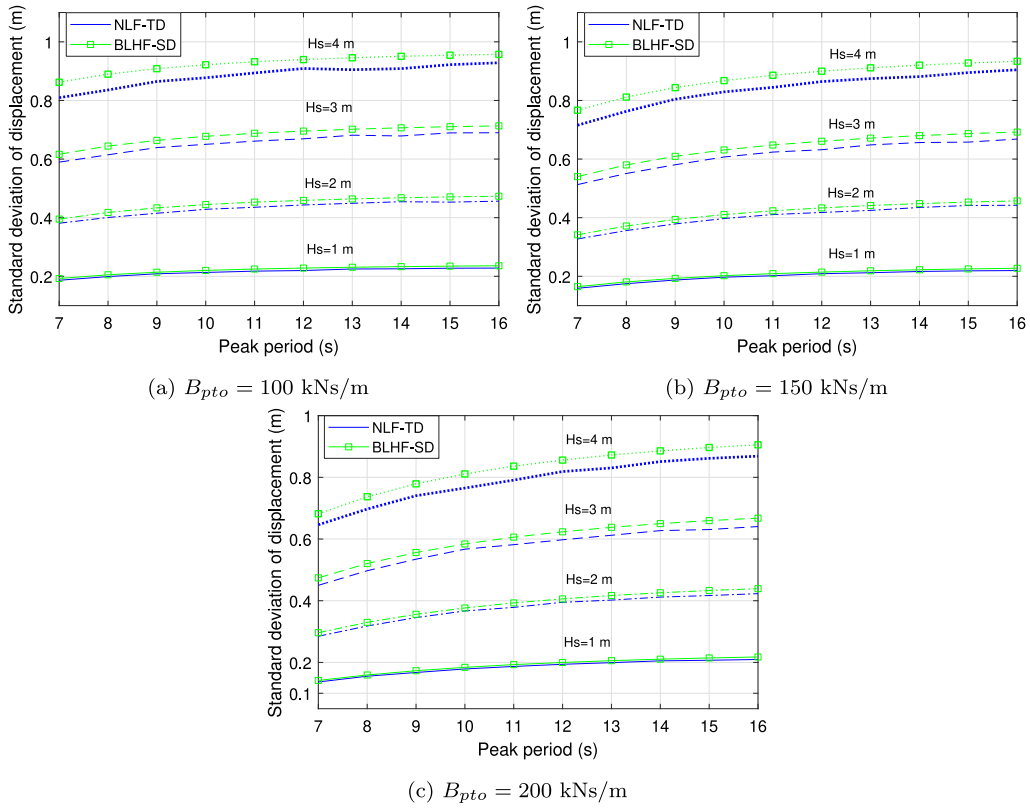
(a) $B_{pto} = 100$ kNs/m

(b) $B_{pto} = 150$ kNs/m

(c) $B_{pto} = 200$ kNs/m

Fig. 6. The standard deviation of the displacement of the WEC with considering different simulation inputs.

defined by the absorbed power divided by the wave power transport per unit of wavefront and the characteristic length of the device (Pecher, 2017). Moreover, the computational efficiency of these models is also quantified for comparison.

5.2.1. Relevance to the sea state

The values of the CWR of the WEC under different significant wave heights are estimated using various models and compared in Fig. 7(a). Additionally, the relative errors of these models with respect to the NHF-TD model are illustrated in Fig. 7(b). It is evident that the differences among these five models are negligible under low significant wave heights, but become more pronounced with increasing significant wave height. Specifically, the LHF-FD model, the SLHF-SD model, and the SBLHF-SD model tend to underestimate the power absorption given the implemented peak period and PTO setting, while the proposed BLHF-SD model results in a slight overestimation. As depicted in Fig. 7(b), modeling accuracy exhibits a clear dependence on significant wave height. For instance, the LHF-FD model demonstrates validity only under strictly mild waves, with its relative error exceeding 10% at significant wave heights of 2.5 m. Conversely, the SLHF-SD model and the SBLHF-SD model yield much lower relative errors, hovering around 10% even as the significant wave height increases to 4 m, where the LHF-FD model reaches a relative error of 20%. In comparison, the BLHF-SD model displays significantly better accuracy than the FD model and the other two previously reported SD models. Although its accuracy is also compromised by increasing significant wave height, it remains below 5% even at significant wave heights as high as 4 m.

The variation of the estimated CWR to the peak period of sea states is presented in Fig. 8. It is seen that the results of the FD model and the two previously reported SD models noticeably deviate from those of the NHF-FD model at low peak periods. Particularly, the relative errors of the LHF-SD model, the SLHF-SD model and the SBLHF-SD model are larger than 10% at the peak period of 6 s. The reason is that the

nonlinearity of the hydrostatic restoring force is more pronounced at low peak periods. This can be further demonstrated by Fig. 9 where the standard deviation of the relative displacement between the buoy and the wave elevation, calculated by the NFL-TD model as the accurate reference, is shown. As observed, the low peak periods correspond to larger relative displacement leading to increased nonlinearity of the hydrostatic restoring force. Besides, depicted in Fig. 9, the relative displacement is limited in long peak periods, resulting in the reduced nonlinearity of the hydrostatic restoring force. Consequently, as shown in Fig. 8, all assessed FD and SD models present good accuracy, with a relative error of less than 5% to the NHF-TD model when the peak period is longer than 10 s. However, it is noteworthy that the relative error of the SBLHF-SD model suggests a tendency to slightly increase from the peak period going beyond 10 s. This results from the applied mean free surface assumption in which the buoy displacement is simply treated as the relative displacement between the buoy and the wave elevation. However, as depicted in Fig. 9, the buoy displacement in long peak periods is remarkably larger than the relative displacement, which makes the SLHF-SD model overestimate the nonlinearity of the hydrostatic restoring force. Comparably, the proposed BLHF-SD model yields results that closely align with those of the NHF-TD model, with a relative error consistently below 3% across all considered peak periods.

5.2.2. Relevance to the PTO parameters

Reactive and passive control stand out as the two primary types of control strategies employed in PTO systems within WECs. In reactive control, both the PTO stiffness and the PTO damping coefficients can be varied to tune the device, and the incorporation of negative stiffness is also feasible. Comparatively, passive control involves the imposition of only the PTO resistance load (damping force). In this work, the relevance of the modeling accuracy to the variation of the PTO damping coefficient and the PTO stiffness coefficient is demonstrated respectively. Throughout each simulation case, the values of the PTO damping and stiffness are initially defined and these values remain
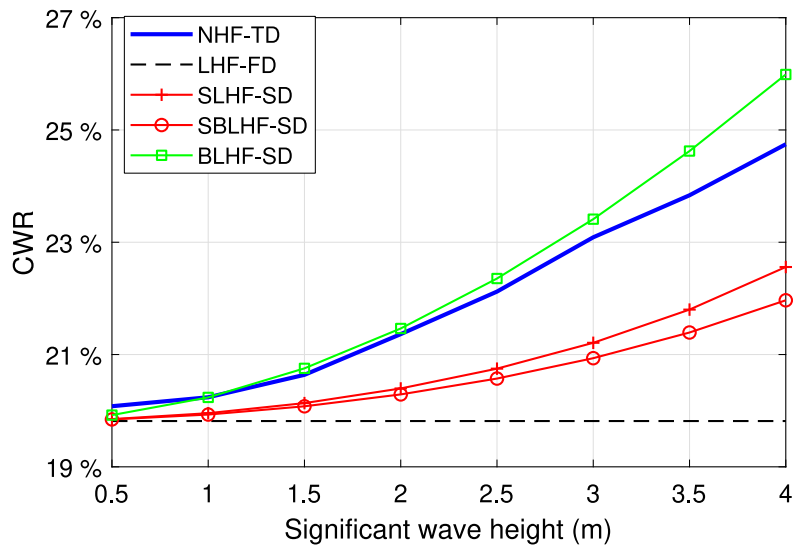
(a) Capture width ratio of the WEC
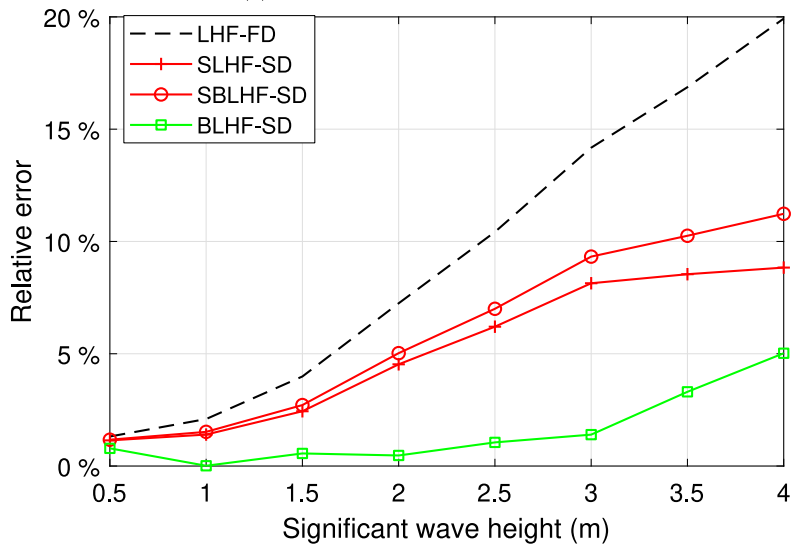
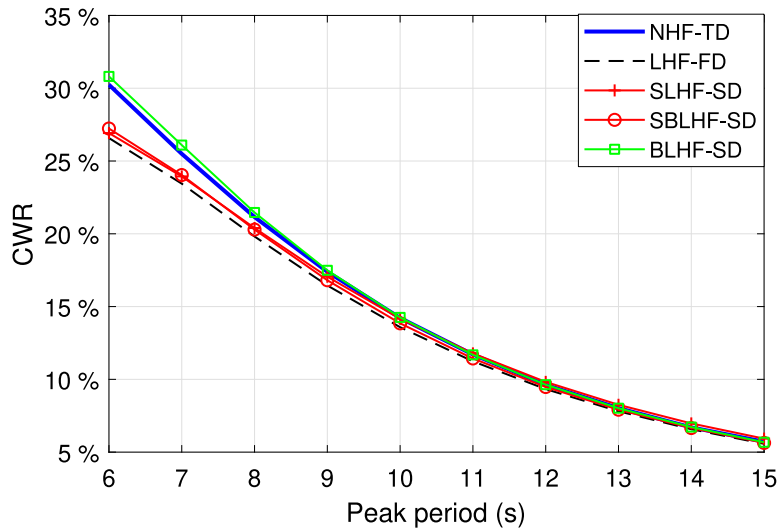(b) The relative errors of the FD and SD modeling to the TD model

Fig. 7. Comparison of capture width ratio predicted by models along different significant wave heights, $T_p = 8.0$ s and $B_{pto} = 150$ kNs/m.

consistent for the entire duration of each sea state in our simulation cases. It is important to note that real-time control strategies can enable instantaneous adjustment of PTO parameters (Ringwood and Bacelli, 2014), while it is not considered here given the scope of this work.

The CWR values of the WEC with various PTO damping coefficients are calculated by different models, as depicted in Fig. 10. It can be seen that the modeling accuracy suggests a strong sensitivity to the PTO damping coefficient. The LHF-FD and SBLHF-SD models' accuracy declines with the increase of the PTO damping. They both result in the underestimation of the CWR. The relative error of the SBLHF-SD model and the LHF-FD model reaches around 15% and 17% when the PTO damping is 300 kNs/m. Comparatively, the SLHF-SD model overestimates the CWR at small PTO damping values, while it leads to underestimation when the PTO damping coefficient becomes larger. Besides, the accuracy of the SLHF-SD model appears low in conditions with small PTO damping values. For instance, the relative error of the SLHF-SD model to the NHF-TD model is even around 19%. It is observed that the relative error of the SLHF-SD model shows a tendency to first decrease with the PTO damping until the PTO damping coefficient reaches approximately 100 kNs/m, then its relative error increases to over 16% at the PTO damping of 300 kNs/m. This can be

explained in such a way that the buoy has relatively less resistance to move, subjected to wave excitation force, with a smaller PTO damping coefficient. In this way, as the buoy dimension of the WEC can be considered small compared to the wavelength given the implemented sea state, the buoy motion tends to follow the wave elevation, which implies a small relative displacement. However, in the SLHF-SD model, the incident wave elevation is neglected, and the buoy motion is simplified as the relative displacement, exaggerating the relative displacement in conditions with small PTO damping coefficients. When the PTO damping is sufficiently large, the SLHF-SD model tends to predict similar results as the LHF-FD model does. This is because the nonlinear hydrostatic effect in the SLHF-SD model is simplified to be only related to the buoy displacement which is, however, negligible due to the large PTO damping coefficients. In this case, the nonlinearity of the hydrostatic restoring force, reflected by the SLHF-SD model, tends to be limited. In comparison, the proposed BLHF-SD model consistently provides close results with the NHF-TD model, in which the relative error is lower than 3% throughout the entire range of considered PTO damping coefficients.

Fig. 11 depicts CWR estimated different models, in which a variety of PTO stiffness coefficients are implemented. It indicates that the

(a) Capture width ratio of the WEC
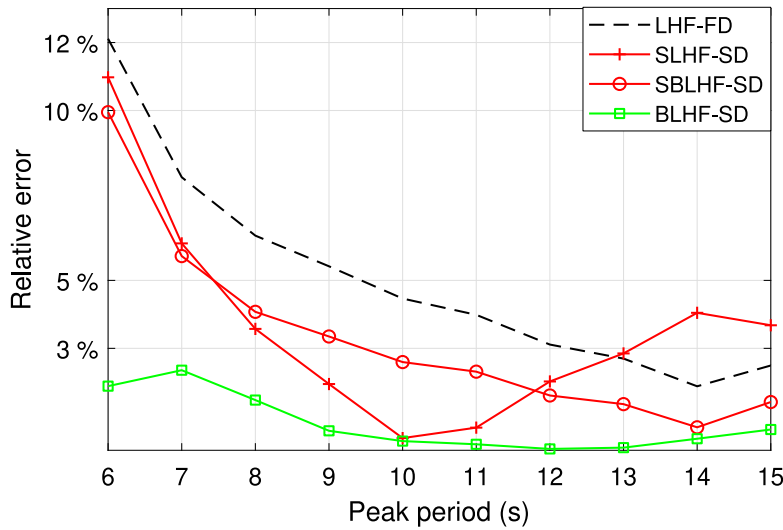
(b) The relative errors of the FD and SD modeling to the TD model

Fig. 8. Comparison of capture width ratio predicted by models along different peak periods, $H_s = 2$ m and $B_{pto} = 150$ kNs/m.
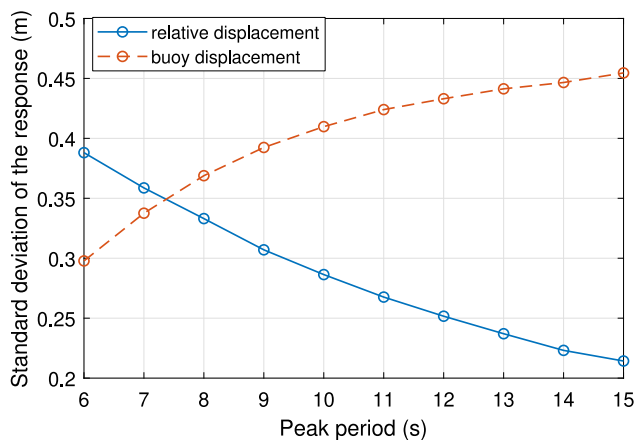

Fig. 9. The standard deviation of the relative displacement between the buoy and the wave elevation and the standard deviation of the buoy displacement, predicted by the NHF-TD model in the conditions of $H_s = 2$ m and $B_{pto} = 150$ kNs/m.

PTO stiffness could hardly affect the accuracy of the proposed BLHF-SD model, and the relative error is strictly within 3% throughout the PTO stiffness ranging from −60 kN/m to 60 kN/m. The LHF-FD model underestimates the CWR, and the discrepancy to the NHF-TD model is the largest among the models. For instance, its relative error is over 12% when the PTO stiffness is −60 kN/m. In addition, the SBLHF-SD model and the SLHF-SD model suggest better accuracy than the LHF-FD model, and their largest relative errors are identified as 7% and 9% in this case.

5.2.3. Relevance to the buoy draft

The buoy draft in the equilibrium position is an important parameter in the design and optimization of WECs since it is directly related to the dynamic property and power performance (Tan et al., 2020, 2022c, 2023a). For buoy geometries with non-uniform cross-sectional areas in the heaving direction, the draft variation is expected to alter the significance of the nonlinear hydrostatic restoring force. To identify the influence of the buoy draft on the accuracy of various models, the estimated CWR values and the corresponding discrepancy relative to the NHF-TD model are calculated for the spherical buoy with five different drafts, as presented in Fig. 12. It is shown in the figure that the accuracy of the LHF-FD model, the SLHF-SD model and the SBLHF-SD
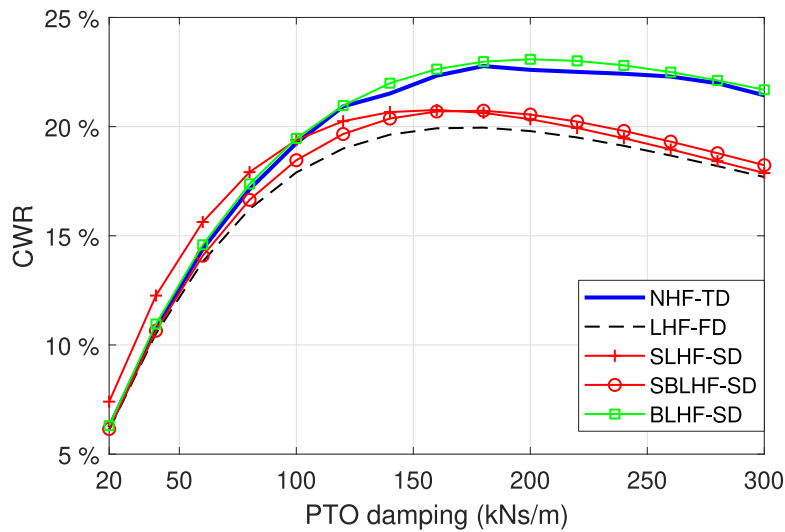
(a) Capture width ratio of the WEC
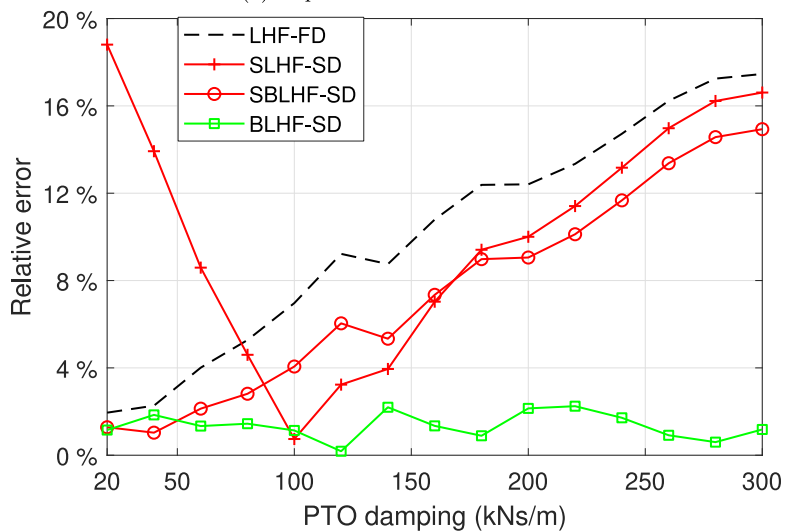
(b) The relative errors of the FD and SD modeling to the TD model

Fig. 10. Comparison of capture width ratio predicted by models along different PTO damping coefficients, $T_p = 8.0$ s and $H_s = 2.5$ m.

model decreases with the increase of the buoy draft. Specifically, the relative error of the LHF-FD model is increased from around 10% at the buoy draft of 2.5 m to 16% at the buoy draft of 3.5 m. Although the two previously proposed SD models, namely the SLHF-SD model and the SBLHF-SD model, demonstrate better modeling accuracy than the LHF-FD model, their relative errors to the BHF-TD model still reach approximately 13% and 12%. However, the accuracy of the BLHF-SD model does not appear strong correlation to the change of the buoy draft, and the relative errors are limited to 3% with a minor overestimation of the CWR.

5.3. Computational efficiency

Table 1 provides an evaluation of the computational efficiencies of various models. To ensure a fair comparison, all models are configured to simulate the WEC under identical operational conditions. Furthermore, all simulations are executed on the same machine, featuring an Intel i7/2.80 GHz processor. It is important to note that only a single-run computational time of the NHF-TD model is presented. However, for performance estimation, multiple runs and the averaging of results are essential to mitigate random errors. While one might argue that extending the simulation period could serve as an alternative

Table 1

Computational efficiency of different modeling approaches ($H_s = 2.5$ m, $T_p = 10$ s and $B_{pto} = 100$ kNs/m.)

Numerical model	Computational time (s)
NHF-TD	5.73 (single run)
LHF-FD	$1.02 \cdot 10^{-3}$
SLHF-SD	$2.92 \cdot 10^{-3}$
SBLHF-SD	$3.22 \cdot 10^{-3}$
BLHF-SD	$4.07 \cdot 10^{-3}$

to running the NHF-TD model multiple times, it is anticipated that the computational time would significantly increase compared to a single-run simulation. Although further discussion on the simulation duration of TD modeling is beyond the scope of this work, additional details on this topic can be found in Anon (2016).

Table 1 indicates that the computational time of the LHF-FD model, the SLHF-SD model, the SBLHF-SD model and the BLHF-SD model increases by sequence, but they all both fall within the same order of magnitude. Notably, the computational time for the TD simulation is markedly higher, with a duration of 5.73 s, over 1000 times that of the proposed BLHF-SD model.
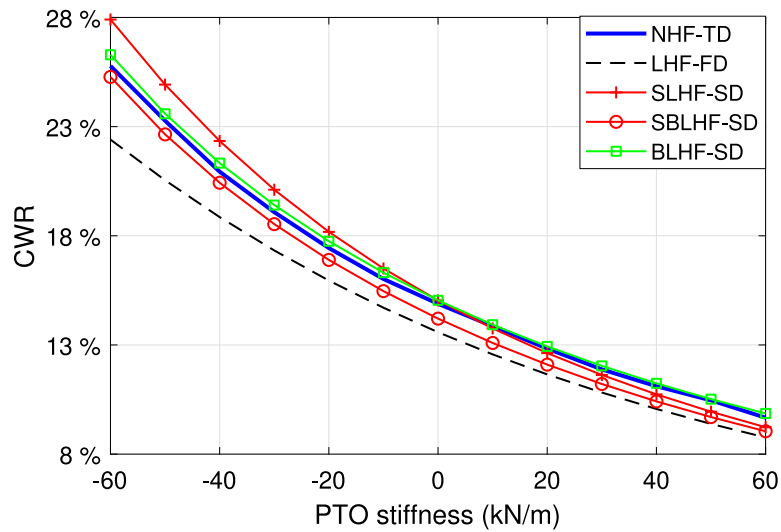
(a) Capture width ratio of the WEC
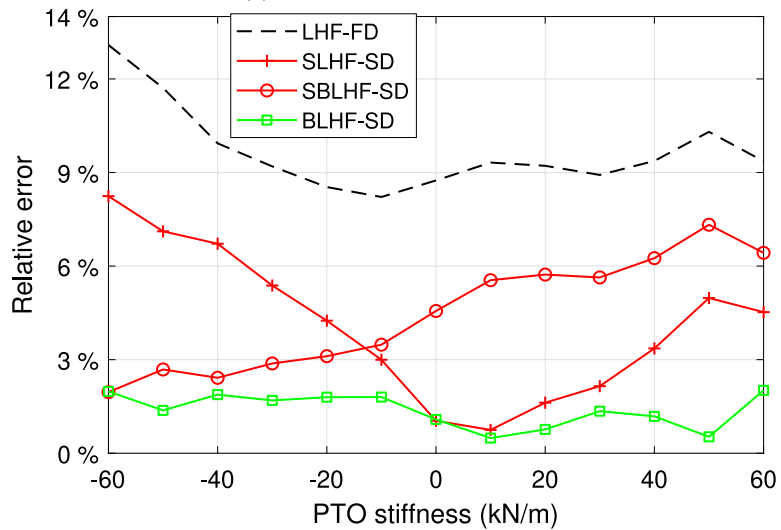
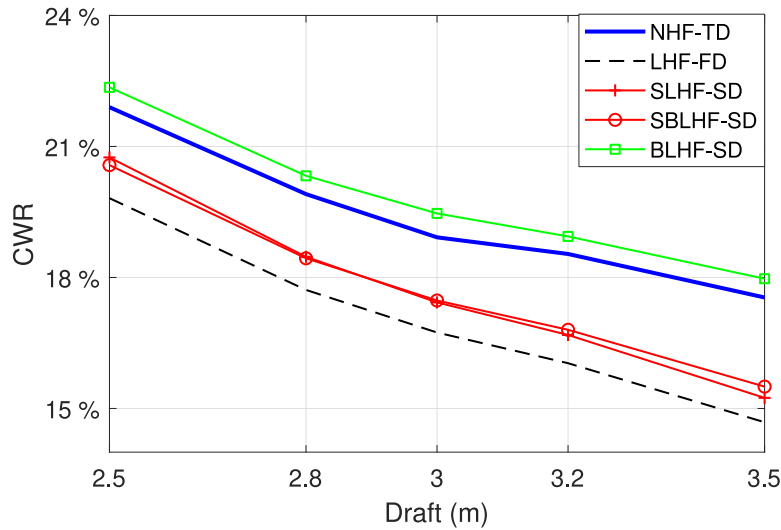(b) The relative errors of the FD and SD modeling to the TD model

Fig. 11. Comparison of capture width ratio predicted by models along different PTO damping, $T_p = 10.0$ s and $H_s = 3$ m. The PTO damping coefficient is 150 kNs/m.
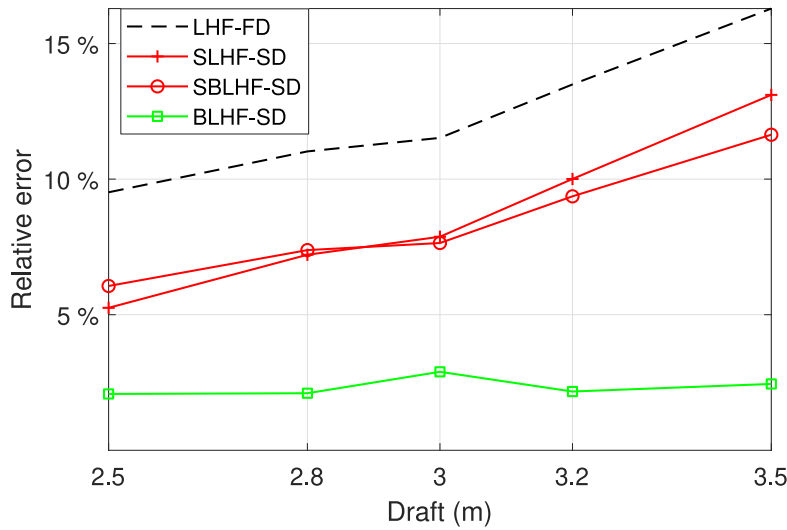
5.4. Discussion

In this work, a modified SD model is proposed to incorporate the nonlinear hydrostatic force of heaving WECs. Adequate accuracy and computational efficiency are observed by comparing the proposed model with the previously developed SD models and the nonlinear TD model. However, it should be noted that the modified SD model is inherently associated with a few limitations which are clarified below.

First, the nonlinear hydrostatic force is the only nonlinear effect considered in this work. This is done deliberately to isolate the influence of other nonlinear sources and better examine the applicability of the modified SD model to this specific nonlinearity. It is thought fair given the purpose of this study, but it should be realized that all results and conclusions are therefore based on the precondition. The implications should be perceived from two aspects. On the one hand, the accuracy of the entire SD modeling approach is expected to decrease with the addition of other sources of nonlinearities. This is because SD modeling is based on the Gaussian assumption, and additional nonlinear effects would inevitably reduce the validity of the Gaussian process in the WEC system, as elaborated in relevant studies (Folley and Whittaker, 2010; Silva et al., 2020). On the other hand, some types of nonlinear effects can become pronounced under

particular circumstances, resulting in significant changes in the overall dynamic behavior of the WEC system. Accordingly, the performance of the modified SD model is expected to differ. For instance, in this work, only an ideal PTO model is implemented. However, in realistic PTO systems, the PTO force or torque could frequently saturate in relatively intense waves, depending on the PTO design. The saturation effect can be interpreted as a reduction in the actual PTO force or torque supplied to the whole system, which tends to amplify the WEC motion. Consequently, even in the identical sea states considered in this study, the intensity of the nonlinear hydrostatic force would inevitably be altered, as it is strongly related to the WEC motion. More generally, similar consequences could arise from various other nonlinear effects in the WEC system, such as nonlinear mooring force, Morison drag term, and Coulomb friction. For those interested in including other nonlinear effects in WECs, detailed information can be found in Folley and Whittaker (2010), Bonfanti and Sirigu (2023), Tan et al. (2022b), Folley and Whittaker (2013), da Silva et al. (2020), Silva et al. (2020). Moreover, the impact of PTO saturation and other nonlinear effects on the accuracy of SD modeling depends on various factors, such as sea states, PTO design, and WEC geometry. It is important to systematically investigate these aspects concerning the performance of SD modeling

(a) Capture width ratio of the WEC

(b) The relative errors of the FD and SD modeling to the TD model

Fig. 12. Comparison of capture width ratio predicted by models along different buoy drafts, $B_{pto} = 150$ kNs/m, $T_p = 10.0$ s and $H_s = 3$ m.

in future work. Nevertheless, extending the discussion further in this direction would deviate from the scope of the current work.

Secondly, the displacement of the WEC is not constrained in the simulations conducted in this work. This implies an assumption that the WEC motion amplitude will not reach unrealistically high levels. The fairness of the assumption is considered acceptable because the study primarily focuses on mild and moderate wave conditions, where SD modeling approach is expected to be highly applicable. However, in more powerful sea states, the motion of the WEC could be significantly greater without displacement limits, making it more likely that the WEC could become fully submerged or leave the water. These phenomena severely challenge the validity of even the nonlinear representation of the hydrostatic force, which thus weakens the reliability of the proposed BLHF-SD model. Fig. 13 shows the time-dependent displacement of the WEC considered in this work, providing insight into the displacement levels relevant to this study. The significant wave height is set to 4 m, the highest value considered in all the simulation cases, and the peak period and PTO damping are defined corresponding to the simulations supporting Fig. 7. Considering the buoy radius as a reference level, it can be seen from Fig. 13 that the WEC motion does not exceed the limit in this particular case. However, this could occur when sea states tend to become more powerful. For more practical applications, such as WEC

design or optimization, it is highly recommended to incorporate an end-stop mechanism in SD modeling, as detailed in Bonfanti and Sirigu (2023), Silva et al. (2020), or to examine the range of displacement achieved by the specific WEC being evaluated to ensure a more realistic outcome.

Thirdly, the numerical models discussed in this study, including the FD models, existing SD models, the BLHF-SD model, and the verification reference NHF-TD model, are all formulated based on linear potential flow theory. This theoretical framework simplifies the fluid to be inviscid, irrotational, and incompressible, thereby neglecting vorticity and viscosity (Falnes, 2003). Consequently, the theory assumes small WEC motions and limited wave steepness. It is known that the method can be extended to cover weakly nonlinear behaviors by including appropriate corrections. For instance, adding nonlinear approximation terms to the Cummins equation or linearized terms to SD modeling can address effects such as viscous drag and nonlinear machinery forces (Babarit et al., 2012; Giorgi and Ringwood, 2017; Penalba and Ringwood, 2016; Folley and Whittaker, 2010; da Silva et al., 2020). However, in extreme sea states, the assumptions of small WEC motion and limited wave steepness tend be severely violated, resulting from significant nonlinear effects such as slamming, wave overtopping, and breaking waves (Fievez and Rafiee, 2015; Shahroozi
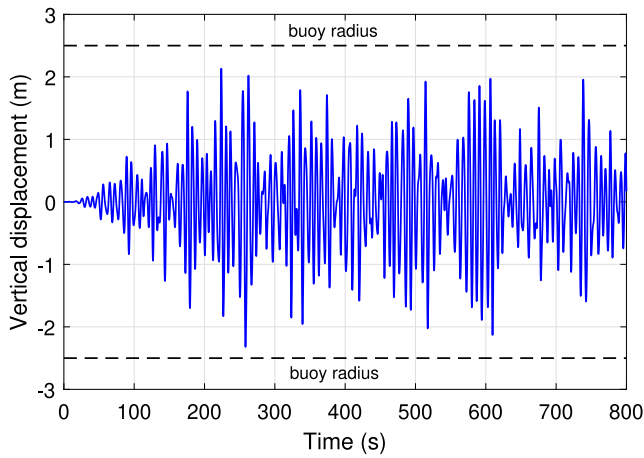
Fig. 13. The time-dependent displacement of the WEC, predicted by the NHF-TD model in the conditions of $T_p = 8$ s, $H_s = 4$ m and $B_{pto} = 150$ kNs/m.

et al., 2022; Tagliafierro et al., 2022). Besides, the increased intensity of these nonlinear effects in extreme events challenges the validity of the Gaussian assumption for both ocean waves and WEC systems, thus weakening the fundamental assumption of stochastic linearization in SD modeling (Folley and Whittaker, 2010). In such scenarios, higher-fidelity approaches become more reasonable than the SD modeling approach. But it should be realized that the majority of energy production by WECs relies on mild and moderate sea states (Lavidas and Blok, 2021b; Babarit et al., 2012), where the proposed BLHF-SD model has suggested satisfactory reliability. Nevertheless, it is of importance to examine the accuracy of the SD modeling when different WEC parameters or operation conditions are implemented. This could contribute to a better perception of the model's applicability and limitations.

6. Conclusion

In this paper, a modified SD model incorporating the nonlinear hydrostatic restoring force is proposed for heaving WECs. Particularly, for better accuracy, the influence of the buoy displacement and the incident wave elevation on the hydrostatic restoring force are collectively considered in the SD model. This is achieved by utilizing the multi-variate stochastic linearization method, and this method is used in the context of SD modeling of WECs for the first time. Using a heaving spherical point absorber as the WEC concept, the proposed BLHF-SD model is verified against the results of the NHF-TD model. Furthermore, an extensive comparison between the proposed BLHF-SD model, previously reported SD models, the LHF-FD model and the NHF-TD model is performed with considering various operation conditions.

First, this work demonstrates the applicability of the multi-variate stochastic linearization method to the construction of SD modeling in WECs. This could facilitate pushing the boundary of SD modeling to include the multi-variate nonlinear effects given the fact that the SD modeling approach is currently highly limited to single-variate stochastic linearization.

Secondly, the modified SD model, namely the BLHF-SD model, exhibits a strong alignment with the NHF-TD model in predicting the power spectral density of the response across a range of frequency components. When considering the standard deviation of the displacement, the difference between the predicted results of the two models appears to be negligible under mild wave conditions. The relative error of the BLHF-SD model compared to the NHF-TD model remains highly constrained, particularly below 4%, even in relatively intense wave states with a significant wave height of 4 m.

Thirdly, in comparison to the SLHF-SD model, the SBLHF-SD model, and the LHF-FD model, the modified BLHF-SD model exhibits enhanced accuracy in estimating the power performance of WECs due to its incorporation of both buoy displacement and incident wave elevation. Within the considered cases in the work, the largest relative error of the proposed BLHF-SD model to the NHF-TD model is only around 5% occurring at a noticeable significant wave height of 4 m. However, the maximum relative error is identified as 20%, 16% and 15% for the LHF-FD model, SLHF-SD model and the SBLHF-SD model. Meanwhile, the modified SBLHF-SD model in this context requires only marginally longer computational time than other SD models, yet remains over one thousand times faster than the NHF-TD model.

Finally, the variability in operational conditions significantly impacts the modeling accuracy of the SLHF-SD model, the SBLHF-SD model, and the LHF-FD model. These models experience a notable decline in accuracy under conditions associated with increased nonlinearity of the hydrostatic restoring force. Specifically, high significant wave heights and short peak periods as wave states, large PTO damping and negative PTO stiffness as PTO parameters, and large buoy drafts lead to reduced accuracy in their modeling results. For instance, within the same wave state, a change in only the PTO damping coefficient could elevate the relative error of the SLHF-SD model, the SBLHF-SD model, and the LHF-FD model from below 3% to over 15%. In contrast, the BLHF-SD model displays minor sensitivity to these factors, exhibiting more stable modeling accuracy associated with a relative error consistently less than 5% throughout the assessed conditions.

CRediT authorship contribution statement

Jian Tan: Writing – review & editing, Writing – original draft, Visualization, Validation, Software, Resources, Methodology, Investigation, Formal analysis, Data curation, Conceptualization. **George Lavidas:** Writing – review & editing, Writing – original draft, Visualization, Validation, Supervision, Software, Resources, Project administration, Methodology, Investigation, Funding acquisition, Formal analysis, Data curation, Conceptualization.

Declaration of competing interest

The authors declare that they have no known competing financial interests or personal relationships that could have appeared to influence the work reported in this paper.

Acknowledgments

Appendix A. Derivation of the linearized coefficient in the SLHF-SD model

In the SLHF-SD model, the hydrostatic restoring force F_{hs} of the spherical buoy is simplified as

$$F_{hs}(z, 0) = \rho g V_{sub}(z, 0) - mg \tag{A.1}$$

Then, the linearized coefficient is calculated as

$$
\begin{aligned}
K_{eq} &= \int_{-\infty}^{\infty} \frac{\partial F_{hs}(z, 0)}{\partial z} p(z) \mathrm{d}z \\
&= \int_{-\infty}^{\infty} -A_{wp}(z, 0) p(z) \mathrm{d}z
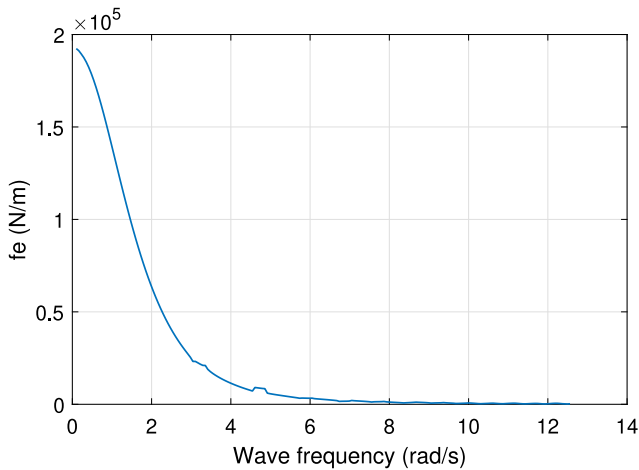\end{aligned}
\tag{A.2}
$$

Fig. D.14. The amplitude of the vertical excitation force coefficient of the semi-submerged spherical buoy.
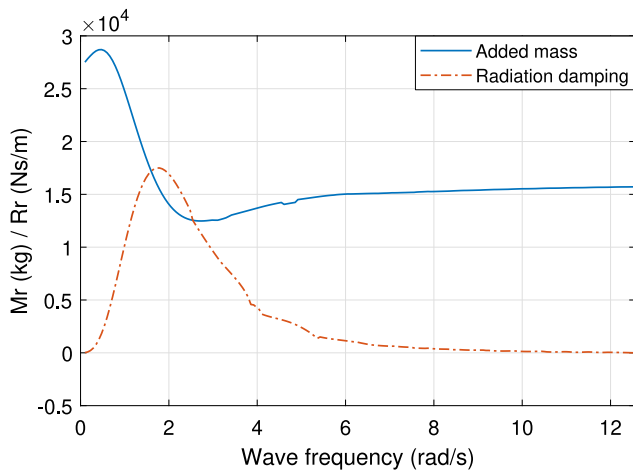

Fig. D.15. The added mass and radiation damping of the semi-submerged spherical buoy in the heaving direction.

where $p(z)$ is the probability density function. Given the Gaussian process, it is expressed as

$$p(z) = \frac{1}{\sigma_z \sqrt{2\pi}} \exp\left(-\frac{z^2}{2\sigma_z^2}\right) \tag{A.3}$$

Substituting (A.3) into (A.2) gives

$$K_{eq} = \pi \rho g (\sigma_z^2 - 2d_0 R + d_0^2) \tag{A.4}$$

Appendix B. Derivation of linearized coefficients in the SBLHF-SD model

In the SBLHF-SD model, the hydrostatic restoring force F_{hs} of the spherical buoy is expressed as

$$F_{hs}(h) = \rho g V_{sub}(h) - \rho g \eta A_{wp}(h) - mg \tag{B.1}$$

It is divided into two parts as

$$F_{hs1}(h) = \rho g V_{sub}(h) - mg \tag{B.2}$$

$$F_{hs2}(\eta, h) = -\rho g \eta A_{wp}(h) \tag{B.3}$$

The linearized coefficient of (B.2) is calculated as

$$\begin{aligned} K_{eq1} &= \langle \frac{\partial F_{hs1}(h)}{\partial h} \rangle \\ &= \rho g \langle \frac{\partial V_{sub}(h)}{\partial h} \rangle \\ &= \langle -\rho g A_{wp}(h) \rangle \end{aligned} \tag{B.4}$$

With the assumption that η is the dominating variable in (B.3) and it is uncorrelated with h, as detailed in the text above (38). The linearized coefficient of (B.3) is then derived as

$$\begin{aligned} K_{eq2} &= \langle \frac{\partial F_{hs2}(\eta)}{\partial \eta} \rangle \\ &= \langle -\rho g A_{wp}(h) \rangle \end{aligned} \tag{B.5}$$

Comparing (B.4) and (B.5), it can be seen that K_{eq1} is equal to K_{eq2}. It is fair to assume that the relative displacement h also follows the Gaussian distribution and its probability density function is given as

$$p(h) = \frac{1}{\sigma_h \sqrt{2\pi}} \exp\left(-\frac{h^2}{2\sigma_h^2}\right) \tag{B.6}$$

Then the solutions of the two expected values can be calculated as

$$\begin{aligned} K_{eq1} = K_{eq2} &= \int_{-\infty}^{\infty} \frac{\partial F_{hs1}(h)}{\partial h} p(h) \mathrm{d}h \\ &= \pi \rho g (\sigma_h^2 - 2d_0 R + d_0^2) \end{aligned} \tag{B.7}$$

Appendix C. Derivation of linearized coefficients in the BLHF-SD model

In the BLHF-SD model, the hydrostatic restoring force is expressed as

$$F_{hs}(z, \eta) = \rho g V_{sub}(z, \eta) - \rho g \eta A_{wp}(z, \eta) - mg \tag{C.1}$$

Applying the multi-variate stochastic linearization method to (C.1) gives the vector of the linearized coefficients as

$$\begin{bmatrix} K_{eq,\eta} \\ K_{eq,z} \end{bmatrix} = \langle \begin{bmatrix} \frac{\partial F_{hs}(z,\eta)}{\partial \eta} \\ \frac{\partial F_{hs}(z,\eta)}{\partial z} \end{bmatrix} \rangle \tag{C.2}$$

where the linearized coefficients $K_{eq,\eta}$ and $K_{eq,z}$ are calculated as

$$K_{eq,\eta} = \int_{-\infty}^{\infty} \int_{-\infty}^{\infty} \frac{\partial F_{hs}(z,\eta)}{\partial \eta} p(z,\eta) \mathrm{d}z \mathrm{d}\eta \tag{C.3}$$

$$K_{eq,z} = \int_{-\infty}^{\infty} \int_{-\infty}^{\infty} \frac{\partial F_{hs}(z,\eta)}{\partial z} p(z,\eta) \mathrm{d}z \mathrm{d}\eta \tag{C.4}$$

where $p(z, \eta)$ embodies the probability density function of the variables z, η. Assuming a joint Gaussian distribution of the two variables, the probability density function is expressed as

$$\begin{aligned} p(z, \eta) = &\frac{1}{2\pi \sigma_z \sigma_\eta \sqrt{1-\gamma^2}} \cdot \\ &\exp\left(-\frac{1}{2\left[1-\gamma^2\right]}\left[\left(\frac{z-\mu_z}{\sigma_z}\right)^2 - 2\rho\left(\frac{z-\mu_z}{\sigma_z}\right)\left(\frac{\eta-\mu_\eta}{\sigma_\eta}\right) + \left(\frac{\eta-\mu_\eta}{\sigma_\eta}\right)^2\right]\right) \end{aligned} \tag{C.5}$$

where $\gamma_{z,\eta}$ is the correlation between the two variables; where μ_z and μ_η are the mean values of z and η respectively. It is reasonable to assume that the wave elevation and the displacement of the buoy satisfy the zero-mean Gaussian distribution, which gives

$$\begin{aligned} \mu_z &= \langle z(t) \rangle = 0 \\ \mu_\eta &= \langle \eta(t) \rangle = 0 \end{aligned} \tag{C.6}$$

Substituting (C.1) and (C.5) into (C.3) and (C.4) gives

$$K_{eq,\eta} = 2\pi \rho g \sigma_\eta^2 - 2\pi \rho g \mathrm{cov}(z, \eta) \tag{C.7}$$

$$K_{eq,z} = \pi \rho g \sigma_z^2 - \pi \rho g \sigma_\eta^2 + \pi \rho g \mathrm{d}_0^2 - 2\pi \rho g \mathrm{Rd}_0 \tag{C.8}$$

where $\text{cov}(z, \eta)$ stands for the covariance of z and η; where σ_η can be related to the significant wave height as

$$\sigma_\eta^2 = \frac{H_s^2}{16} \tag{C.9}$$

According to Hartmann (2016), the covariance can be calculated in the frequency domain as

$$\text{cov}(z, \eta) = \sum_{j=1}^{N} \text{Re}\{\hat{\sigma}_{z,\eta}(\omega_j)\} \Delta\omega \tag{C.10}$$

where $\sigma_{z,\eta}$ represents the cross-spectrum of variables z and η, and $S_{\hat{\eta}(\omega_j)}$ stands for the power spectral density of the incident wave elevation. As demonstrated in Hartmann (2016), the cross-spectrum can be calculated as

$$\hat{\sigma}_{z,\eta}(\omega_j) = \frac{\hat{z}(\omega_j)}{\hat{\eta}(\omega_j)} S_{\hat{\eta}(\omega_j)} \tag{C.11}$$

where superscription $*$ embodies the complex conjugate of the value. The correlation can then be given as

$$\gamma_{z,\eta} = \frac{\text{cov}(z, \eta)}{\sigma_z \sigma_\eta} \tag{C.12}$$

Appendix D. Hydrodynamic coefficients

As inputs to the FD, SD and TD models, the hydrodynamic coefficients of the WEC calculated by Nemoh are presented in Figs. D.14 and D.15.

References

Anon, 2016. Numerical Modelling of Wave Energy Converters.

Babarit, A., Hals, J., Muliawan, M.J., Kurniawan, A., Moan, T., Krokstad, J., 2012. Numerical benchmarking study of a selection of wave energy converters. Renew. Energy 41, 44–63.

Bonfanti, M., Giorgi, G., 2022. Improving computational efficiency in WEC design: Spectral-domain modelling in techno-economic optimization. J. Mar. Sci. Eng. 10 (10), 1468.

Bonfanti, M., Sirigu, S.A., 2023. Spectral-domain modelling of a non-linear wave energy converter: Analytical derivation and computational experiments. Mech. Syst. Signal Process. 198, 110398.

Brahma, S., Ossareh, H.R., 2018. Stochastic linearization of multivariate nonlinearities. arXiv preprint arXiv:1807.06135.

Brahma, S., Ossareh, H.R., 2021. Stochastic linearization of feedback systems with multivariate nonlinearities and systems with state-multiplicative noise. IEEE Trans. Autom. Control 67 (6), 3141–3148.

Coe, R.G., Bull, D.L., 2015. Sensitivity of a wave energy converter dynamics model to nonlinear hydrostatic models. In: International Conference on Offshore Mechanics and Arctic Engineering, vol. 56574, American Society of Mechanical Engineers, V009T09A030.

Cummins, W., Iiuhl, W., Uinm, A., 1962. The Impulse Response Function and Ship Motions. Citeseer.

Falnes, J., 2003. Ocean waves and oscillating systems. Ocean Engineering, vol. 30, (no. 7), p. 953.

Fievez, J., Rafiee, A., 2015. Numerical Prediction of Extreme Loads on the CETO Wave Energy Converter. In: Proceedings of the 11th European Wave and Tidal Energy Conference. (no. September).

Folley, M., 2016. Numerical Modelling of Wave Energy Converters: State-Of-The-Art Techniques for Single Devices and Arrays. Academic Press.

Folley, M., Whittaker, T., 2010. Spectral modelling of wave energy converters. Coast. Eng. 57 (10), 892–897.

Folley, M., Whittaker, T., 2013. Validating a spectral-domain model of an OWC using physical model data. Int. J. Mar. Energy 2, 1–11.

Giorgi, G., Penalba, M., Ringwood, J., 2016. Nonlinear hydrodynamic models for heaving buoy wave energy converters.

Giorgi, G., Ringwood, J.V., 2017. Nonlinear Froude-Krylov and viscous drag representations for wave energy converters in the computation/fidelity continuum. Ocean Eng. 141, 164–175.

Giorgi, G., Ringwood, J.V., 2018a. Analytical representation of nonlinear Froude-Krylov forces for 3-DoF point absorbing wave energy devices. Ocean Eng. 164, 749–759.

Giorgi, G., Ringwood, J.V., 2018b. Comparing nonlinear hydrodynamic forces in heaving point absorbers and oscillating wave surge converters. J. Ocean Eng. Mar. Energy 4 (1), 25–35.

Guillou, N., Lavidas, G., Chapalain, G., 2020. Wave energy resource assessment for exploitation—A review. J. Mar. Sci. Eng. 8 (9), 705.

Gunawardane, S., Folley, M., Sanjaya, S., 2017. Spectral-domain modelling of the non-linear hydrostatic stiffness of a heaving-sphere wave energy converter. In: Proceedings of the 28th International Symposium on Transport Phenomena, Peradeniya, Sri Lanka. pp. 22–24.

Guo, B., Ringwood, J.V., 2021. A review of wave energy technology from a research and commercial perspective. IET Renew. Power Gener. 15 (14), 3065–3090.

Hartmann, D., 2016. ATM 552 Course Notes: Time Series Analysis. University of Washington.

Ji, X., Al Shami, E., Monty, J., Wang, X., 2020. Modelling of linear and non-linear two-body wave energy converters under regular and irregular wave conditions. Renew. Energy 147, 487–501.

Jin, S., Greaves, D., 2021. Wave energy in the UK: Status review and future perspectives. Renew. Sustain. Energy Rev. 143, 110932.

Lavidas, G., Blok, K., 2021a. Levelised cost of electricity for wave energy converters and the perception of milder resource non-viability in the north sea. In: Proceedings of the 14th European Wave and Tidal Energy Conference.

Lavidas, G., Blok, K., 2021b. Shifting wave energy perceptions: The case for wave energy converter (WEC) feasibility at milder resources. Renew. Energy 170, 1143–1155.

Lavidas, G., Venugopal, V., 2017. A 35 year high-resolution wave atlas for nearshore energy production and economics at the Aegean sea. Renew. Energy 103, 401–417.

Lawson, M., Yu, Y.-H., Nelessen, A., Ruehl, K., Michelen, C., 2014a. Implementing nonlinear buoyancy and excitation forces in the wec-sim wave energy converter modeling tool. In: International Conference on Offshore Mechanics and Arctic Engineering, vol. 45547, American Society of Mechanical Engineers, V09BT09A043.

Lawson, M., Yu, Y.-H., Ruehl, K., Michelen, C., et al., 2014. Development and demonstration of the WEC-sim wave energy converter simulation tool.

Li, Y., Yu, Y.H., 2012. A synthesis of numerical methods for modeling wave energy converter-point absorbers. Renew. Sustain. Energy Rev. 16 (6), 4352–4364.

Martinez, A., Iglesias, G., 2022. Mapping of the levelised cost of energy for floating offshore wind in the European Atlantic. Renew. Sustain. Energy Rev. 154, 111889.

Pastor, J., Liu, Y., 2014. Frequency and time domain modeling and power output for a heaving point absorber wave energy converter. Int. J. Energy Environ. Eng. 5 (2–3), 1–13.

Pecher, A., 2017. Handbook of Ocean Wave Energy. vol. 7.

Penalba, M., Kelly, T., Ringwood, J., 2017. Using NEMOH for Modelling Wave Energy Converters : A Comparative Study with WAMIT. In: 12th European Wave and Tidal Energy Conference. p. 10.

Penalba, M., Ringwood, J.V., 2016. A review of wave-to-wire models for wave energy converters. Energies 9 (7).

Penalba Retes, M., Giorgi, G., Ringwood, J., 2015. A review of non-linear approaches for wave energy converter modelling. In: Proceedings of the 11th European Wave and Tidal Energy Conference. European Wave and Tidal Energy Conference 2015.

Pérez, T., Fossen, T., 2008. Time-vs. frequency-domain identification of parametric radiation force models for marine structures at zero speed. Model. Identif. Control 29 (1), 1–19.

Prado, M., Polinder, H., 2013. Direct drive wave energy conversion systems: An introduction. In: Electrical Drives for Direct Drive Renewable Energy Systems. Woodhead Publishing Limited, pp. 175–194.

Ransley, E., Greaves, D., Raby, A., Simmonds, D., Hann, M., 2017. Survivability of wave energy converters using CFD. Renew. Energy 109, 235–247.

Ricci, P., António, A.F., Saulnier, J.B., Pontes, M.T., 2008. Time-domain models and wave energy converters performance assessment. Proc. Int. Conf. Offshore Mech. Arctic Eng. - OMAE 6 (May 2015), 699–708.

Ringwood, J.V., Bacelli, G., 2014. Control of Wave-Energy Converters. (no. October).

Roberts, J.B., Spanos, P.D., 2003. Random Vibration and Statistical Linearization. Courier Corporation.

Shahroozi, Z., Göteman, M., Engström, J., 2022. Experimental investigation of a point-absorber wave energy converter response in different wave-type representations of extreme sea states. Ocean Eng. 248, 110693.

Silva, L.S.P.d., 2019. Nonlinear Stochastic Analysis of Wave Energy Converters Via Statistical Linearization (Ph.D. thesis). Universidade de São Paulo.

da Silva, L.S., Cazzolato, B.S., Sergiienko, N.Y., Ding, B., Morishita, H.M., Pesce, C.P., 2020. Statistical linearization of the Morison's equation applied to wave energy converters. J. Ocean Eng. Mar. Energy 6, 157–169.

Silva, L., Sergiienko, N., Pesce, C., Ding, B., Cazzolato, B., Morishita, H., 2020. Stochastic analysis of nonlinear wave energy converters via statistical linearization. Appl. Ocean Res. 95, 102023.

Soukissian, T., O'Hagan, A.M., Azzellino, A., Boero, F., Brito e Melo, A., Comiskey, P., Gao, Z., Howell, D., Le Boulluec, M., Maisondieu, C., et al., 2023. European Offshore Renewable Energy: Towards a Sustainable Future. European Marine Board.

Spanos, P.D., Strati, F.M., Malara, G., Arena, F., 2018. An approach for non-linear stochastic analysis of U-shaped OWC wave energy converters. Probab. Eng. Mech. 54, 44–52.

Tagliafierro, B., Martínez-Estévez, I., Domínguez, J.M., Crespo, A.J., Göteman, M., Engström, J., Gómez-Gesteira, M., 2022. A numerical study of a taut-moored point-absorber wave energy converter with a linear power take-off system under extreme wave conditions. Appl. Energy 311, 118629.

Tan, J., Jarquin Laguna, A., Polinder, H., Miedema, S., 2022a. The application of the spectral domain modeling to the techno-economic analysis of the adjustable draft point absorbers. In: International Conference on Offshore Mechanics and Arctic Engineering, vol. 85932, American Society of Mechanical Engineers, V008T09A067.

Tan, J., Laguna, A.J., 2023. Spectral-domain modelling of wave energy converters as an efficient tool for adjustment of PTO model parameters. In: Proceedings of the European Wave and Tidal Energy Conference, vol. 15.

Tan, J., Polinder, H., Laguna, A.J., Miedema, S., 2022b. The application of the spectral domain modeling to the power take-off sizing of heaving wave energy converters. Appl. Ocean Res. 122, 103110.

Tan, J., Polinder, H., Laguna, A.J., Miedema, S., 2022c. A numerical study on the performance of the point absorber wave energy converter integrated with an adjustable draft system. Ocean Eng. 254, 111347.

Tan, J., Polinder, H., Laguna, A.J., Miedema, S., 2023a. A wave-to-wire analysis of the adjustable draft point absorber wave energy converter coupled with a linear permanent-magnet generator. Ocean Eng. 276, 114195.

Tan, J., Polinder, H., Laguna, A.J., Wellens, P., Miedema, S.A., 2021a. The influence of sizing of wave energy converters on the techno-economic performance. J. Mar. Sci. Eng. 9 (1), 52.

Tan, J., Polinder, H., Wellens, P., Miedema, S., 2020. A feasibility study on downsizing of power take off system of wave energy converters. In: Developments in Renewable Energies Offshore. CRC Press, pp. 140–148.

Tan, J., Tao, W., Laguna, A.J., Polinder, H., Xing, Y., Miedema, S., 2023b. A spectral-domain wave-to-wire model of wave energy converters. Appl. Ocean Res. 138, 103650.

Tan, J., Wang, X., Jarquin Laguna, A., Polinder, H., Miedema, S., 2021b. The influence of linear permanent magnet generator sizing on the techno-economic performance of a wave energy converter. In: 2021 13th International Symposium on Linear Drives for Industry Applications. LDIA, pp. 1–6.

Tan, J., Wang, X., Polinder, H., Laguna, A.J., Miedema, S.A., 2022d. Downsizing the linear PM generator in wave energy conversion for improved economic feasibility. J. Mar. Sci. Eng. 10 (9), 1316.

Taveira-Pinto, F., Rosa-Santos, P., Fazeres-Ferradosa, T., 2020. Marine renewable energy. Renew. Energy 150, 1160–1164.

Wolgamot, H.A., Fitzgerald, C.J., 2015. Nonlinear hydrodynamic and real fluid effects on wave energy converters. Proc. Inst. Mech. Eng. A 229 (7), 772–794.

Zurkinden, A.S., Ferri, F., Beatty, S., Kofoed, J.P., Kramer, M., 2014. Non-linear numerical modeling and experimental testing of a point absorber wave energy converter. Ocean Eng. 78, 11–21.